Regulation of blood–brain barrier integrity by microbiome-associated methylamines and cognition by trimethylamine *N*-oxide

Lesley Hoyles[1]*, Matthew G. Pontifex[2], Ildefonso Rodriguez-Ramiro[2,3], M. Areeb Anis-Alavi[4], Khadija S. Jelane[4], Tom Snelling[5], Egle Solito[6,7], Sonia Fonseca[8], Ana L. Carvalho[8], Simon R. Carding[2,8], Michael Müller[2], Robert C. Glen[5,9] David Vauzour[2] & Simon McArthur[4]*

[1]Department of Biosciences, School of Science and Technology, Nottingham Trent University, Clifton, Nottingham, UK

[2]Norwich Medical School, University of East Anglia, Norwich, UK

[3]Metabolic Syndrome Group, Madrid Institute for Advanced Studies (IMDEA) in Food, Madrid, E28049, Spain

[4]Institute of Dentistry, Barts & the London School of Medicine & Dentistry, Blizard Institute, Queen Mary University of London, London, UK

[5]Faculty of Medicine, Department of Metabolism, Digestion and Reproduction, Imperial College London, London, UK

[6]William Harvey Research Institute, Barts & the London School of Medicine & Dentistry, Queen Mary, University of London, London, UK

[7]Dipartimento di Medicina molecolare e Biotecnologie mediche, Federico II University, Naples, Italy

[8]The Gut Microbes and Health Research Programme, The Quadram Institute, Norwich Research Park, Norwich, UK

[9]Centre for Molecular Informatics, Department of Chemistry, University of Cambridge, Cambridge, UK

***Corresponding authors:** Lesley Hoyles, lesley.hoyles@ntu.ac.uk; Simon McArthur, s.mcarthur@qmul.ac.uk

Keywords: Trimethylamine *N*-oxide, trimethylamine, blood–brain barrier, cognition

ABSTRACT

Background

Communication between the gut microbiota and the brain is primarily mediated *via* soluble microbe-derived metabolites, but the details of this pathway remain poorly defined. Methylamines produced by microbial metabolism of dietary choline and L-carnitine have received attention due to their proposed association with vascular disease, but their effects upon the cerebrovascular circulation have hitherto not been studied.

Results

Here we use an integrated *in vitro*/*in vivo* approach to show that physiologically relevant concentrations of the dietary methylamine trimethylamine *N*-oxide (TMAO) enhanced blood-brain barrier (BBB) integrity and protected it from inflammatory insult, acting through the tight junction regulator annexin A1. In contrast, the TMAO precursor trimethylamine (TMA) impaired BBB function and disrupted tight junction integrity. Moreover, we show that long-term exposure to TMAO protects murine cognitive function from inflammatory challenge, acting to limit astrocyte and microglial reactivity in a brain region-specific manner.

Conclusion

Our findings demonstrate the mechanisms through which microbiome-associated methylamines directly interact with the mammalian BBB, with consequences for cerebrovascular and cognitive function.

INTRODUCTION

As the role of the gut microbiota in host physiology and disease is categorised, novel pathways through which these interactions are mediated continue to emerge. We and others recently identified the blood–brain barrier (BBB) as a target for gut microbe-derived short-chain fatty acid (SCFA) activity, with butyrate and propionate acting to promote BBB integrity and protect the cerebral vasculature from insult [1,2]. SCFAs represent just one of many classes of gut microbe-derived metabolites, with little known as to how these other classes may influence BBB function.

Dietary methylamines, such as choline, phosphatidylcholine, betaine and trimethylamine-*N*-oxide (TMAO), are a class of metabolites receiving considerable attention as modulators of vascular function [3,4], although the mechanism(s) by which they affect human physiology remain poorly understood. The aforementioned methylamines can be broken down by members of the gut microbiota into trimethylamine (TMA) [5], which is carried from the gut through the portal vasculature to the liver and rapidly converted into TMAO by flavin monooxygenases [6]. TMAO then enters the systemic circulation, reaching fasting plasma concentrations of between 2 and 40 μM in humans [7–9], prior to excretion through the urine [5]. Approximately ten-fold lower concentrations of TMA compared with TMAO are found in the circulation under normal physiological conditions.

Early observational work reported an association between atherosclerosis and elevated levels of TMAO [10,11]. Similarly, pre-clinical studies demonstrate the damaging effects of supraphysiological TMAO doses in atherosclerosis-prone mice [12] and upon thrombus formation [13]. Despite this, the impact of TMAO upon the vasculature remains uncertain, with a number of detailed studies encompassing both human and murine systems having failed to replicate these initial findings [14], instead suggesting that this negative relationship disappears upon correction for renal function [4,15–17] and thus indicating that raised TMAO levels may in fact reflect impaired excretion rather than being a causative factor in disease. Moreover, protective roles for TMAO have been reported in rodent models of hypertension [18], atherosclerosis [19] and non-alcoholic steatohepatitis [20] and we have previously shown TMAO to improve glucose homeostasis and insulin secretion in mice fed a high-fat diet [21]. Perhaps helping to clarify this apparent contradiction, recent studies have established that intravenous treatment of rats with the TMAO precursor TMA, but not TMAO itself, increases mean arterial blood pressure [22]. Notably, the majority of reports describing associations of plasma TMAO with cardiovascular disease have not concurrently monitored levels of TMA; TMA but not TMAO has been shown to associate with severe aortic stenosis [22] and gestational diabetes risk [23].

Beyond vascular health, dietary methylamines have implications for cognition, with a positive correlation observed between choline intake and cognitive function in both humans [24,25] and mice [26,27]. In contrast, cerebrospinal fluid TMAO levels have been indicated as predictive of cognitive decline in Alzheimer's disease [28], while suppression of microbial TMA/TMAO production improves cognitive function in the murine APP/PS1 model of Alzheimer's disease [29]. Given the disparities in the literature regarding the effects of methylamines upon the vasculature, and our increasing awareness of the BBB as a major actor in the pathology of multiple neurological conditions, we investigated the effects of physiologically relevant concentrations of TMAO and its precursor TMA upon BBB integrity and cognitive behaviour.

102 **METHODS**

103

104 *Endothelial cell culture*

105 The human cerebromicrovascular endothelial cell line hCMEC/D3 was maintained and treated
106 as described previously [2,30]. Cells bearing shRNA sequences targeting annexin A1
107 (*ANXA1*) or non-specific scramble sequences were produced as described previously [31];
108 the degree of *ANXA1* knock-down was confirmed by flow cytometry analysis (Suppl. Fig. 1).
109 For all lines, cells were cultured to confluency in complete EBM-2MV microvascular
110 endothelial cell growth medium (Promocell GmbH, Heidelberg, Germany), whereupon
111 medium was replaced by EBM-2MV without VEGF and cells were further cultured for a
112 minimum of 4 days to enable intercellular tight junction formation prior to experimentation.

113

114 *In vitro barrier function assessments*

115 Paracellular permeability and transendothelial electrical resistance (TEER) were measured on
116 100 % confluent hCMEC/D3 cultures polarised by growth on 24-well plate polyethylene
117 terephthalate (PET) transwell inserts (surface area: 0.33 cm^2, pore size: 0.4 µm; Greiner Bio-
118 One GmbH, Kremsmünster, Austria) coated with calf-skin collagen and fibronectin (Sigma-
119 Aldrich, UK). The permeability of hCMEC/D3 cell monolayers to 70 kDa FITC-dextran (2
120 mg/ml) was measured as described previously [31–33]. TEER measurements were performed
121 using a Millicell ERS-2 Voltohmmeter (Millipore, Watford, UK) and were expressed as $\Omega.cm^2$.
122 In all cases, values obtained from cell-free inserts similarly coated with collagen and
123 fibronectin were subtracted from the total values. In some cases, barrier integrity was tested
124 by challenge with bacterial lipopolysaccharide (LPS). Confluent hCMEC/D3 monolayers were
125 treated with TMAO or TMA for 12 h, whereupon LPS (*Escherichia coli* O111:B4; 50 ng/ml,
126 comparable to circulating levels of LPS in human endotoxemia [34]) was added for a further
127 12 h, without wash-out. Barrier function characteristics were then interrogated as described
128 above.

129

130 *Cell adhesion assays*

131 hCMEC/D3 cells were cultured to confluency on transwell inserts (0.4 µm pore size, 0.33 cm^2
132 diameter, Greiner Bio-One Gmbh, Austria) prior to 16 h treatment with 10 ng/ml TNFα.
133 Monolayers were then incubated for 2 h with U937 monocytic cells pre-labelled according to
134 manufacturer's instructions with CMFDA cell tracker dye (ThermoFisher Scientific, UK). Co-
135 cultures were washed vigorously with ice-cold PBS three times and fixed by incubation for 10
136 min in 1 % formaldehyde in 0.1 M PBS. Co-cultures were mounted and examined using an
137 Axiovert 200M inverted microscope (Zeiss) equipped with a 20x objective lens. Images were

138 captured with ZEN imaging software (Carl Zeiss Ltd, UK) and analysed using ImageJ 1.53c
139 (National Institutes of Health, USA).
140
141 *Microarrays*
142 hCMEC/D3 cells were grown on 6-well plates coated with calf-skin collagen (Sigma-Aldrich,
143 Gillingham, UK), and collected in TRIzol (Thermo-Fisher Scientific, UK) as described
144 previously [2]. Total RNA was extracted using a TRIzol Plus RNA purification kit (Thermo-
145 Fisher Scientific, UK) and quantified using a CLARIOstar spectrophotometer equipped with
146 an LVis microplate (BMG Labtech GmbH, Germany).
147
148 Hybridization experiments were performed by Macrogen Inc. (Seoul, Republic of Korea) using
149 Illumina HumanHT-12 v4.0 Expression BeadChips (Illumina Inc., San Diego, CA) as described
150 previously [2].
151
152 *Processing and analyses of array data*
153 Raw data supplied by Macrogen were quality-checked, log_2-transformed and loess-
154 normalized (2 iterations) using affy [35]. Probe filtering and matching of probes not classified
155 as 'Bad' or 'No match' to Entrez identifiers were done as described previously [2]. Average
156 gene expression values were used for identification of differentially expressed genes. Array
157 data have been deposited in ArrayExpress under accession number E-MTAB-6662.
158 Normalized data are available (Supplementary Table 1).
159
160 Enrichr [36,37] was used to perform Gene Ontology (GO) analysis. Signaling Pathway Impact
161 Analysis (SPIA) was used to determine whether Kyoto Encyclopedia of Genes and Genomes
162 (KEGG) pathways were activated or inhibited in hCMEC/D3 cells exposed to TMAO or TMA
163 [38]. Human KEGG pathways (KGML format) downloaded from the KEGG PATHWAY
164 database [39] were used for network (KEGGgraph, RBGL [40]) analysis.
165
166 *Immunofluorescence microscopy*
167 hCMEC/D3 cells were cultured on 24-well plate PET transwell inserts (surface area: 0.33 cm^2,
168 pore size: 0.4 µm; Greiner Bio-One GmbH, Kremsmünster, Austria) coated with calf-skin
169 collagen and fibronectin (Sigma-Aldrich, UK), prior to immunostaining according to standard
170 protocols [2,31] and using a primary antibody directed against zonula occludens-1 (ZO-1;
171 1:100, ThermoFisher Scientific, UK) or Alexafluor 488-conjugated phalloidin (1:140,
172 ThermoFisher Scientific, UK). Nuclei were counterstained with DAPI (Sigma-Aldrich, UK).
173 Images were captured using an LSM880 confocal laser scanning microscope (Carl Zeiss Ltd,
174 Cambridge, UK) fitted with 405 nm and 488 nm lasers, and a 63x oil immersion objective lens

175 (NA, 1.4 mm, working distance, 0.17 mm). Images were captured with ZEN imaging software
176 (Carl Zeiss Ltd, UK) and analysed using ImageJ 1.53c (National Institutes of Health, USA).
177
178 *Flow cytometry analysis*
179 Following experimental treatment, hCMEC/D3 cells were detached using 0.05 % trypsin and
180 incubated with an unconjugated rabbit polyclonal antibody directed against ANXA1 (1:1000,
181 ThermoFisher Scientific, UK) on ice for 30 min, followed by incubation with an AF488-
182 conjugated goat anti-rabbit secondary antibody (1:500, ThermoFisher Scientific, UK). Similarly
183 detached hCMEC/D3 cells were incubated with APC-conjugated mouse monoclonal anti-
184 BCRP (1:100, BD Biosciences, Oxford, UK), or PE-conjugated mouse monoclonal anti-
185 MDR1A (1:100, BD Biosciences, UK) antibodies on ice for 30 min, alongside fluorescence
186 minus one controls. Immunofluorescence was analysed for 20,000 events per treatment using
187 a BD FACSCanto II (BD Biosciences, UK) flow cytometer; data were analysed using FlowJo
188 8.0 software (Treestar Inc., CA, USA).
189
190 *Efflux transporter assays*
191 Activity of the major efflux transporters P-glycoprotein and Breast Cancer Resistance Protein
192 (BCRP) was determined through the use of commercially available assays (PREDEASY™
193 ATPase Assay Kits, Solvo Biotechnology Inc., Budapest, Hungary), performed according to
194 the manufacturer's instructions. Stepwise dose–response curves centred around reported
195 physiological circulating concentrations of TMA (4.9 nM – 10.8 μM) and TMAO (0.5 μM – 1.08
196 mM) were constructed ($n = 4$) to investigate inhibitory effects of the methylamines upon
197 transporter activity.
198
199 *ELISA*
200 Culture medium ANXA1 content was assayed by specific ELISA as described previously [41].
201 Serum TNFα and IL-1β concentrations were assayed using commercial ELISA kits according
202 to the manufacturer's instructions (ThermoFisher Scientific, UK).
203
204 *Animal experiments*
205 All animal experiments were performed according to the UK Animals (Scientific Procedures)
206 Act of 1986, under UK Home Office Project Licences PFA5C4F4F (short term studies) and
207 70/8710 (long term studies), following ethical review by the Animal Welfare and Ethical Review
208 Boards of Queen Mary, University of London or the University of East Anglia, respectively.
209 Wild-type male C57Bl/6J mice (Charles River Ltd, Harlow, UK) aged 8 weeks at the start of
210 procedures were used throughout, with a group size of n=5-6 for short term studies and n=8
211 for long-term/behavioural analyses. Animals were housed in individually ventilated cages on

212 a daily 12 h:12 h light/dark cycle with, unless otherwise indicated, *ad libitum* access to
213 standard mouse chow and drinking water. Experimental procedures were started at 9 am to
214 minimise variation associated with circadian rhythms.
215
216 *Assessment of acute effects of TMAO on BBB integrity*
217 Mice (n=5-6 per group) were injected intraperitoneally (i.p.) with 1.8 mg/kg body weight TMAO
218 in 100 µl saline vehicle, a dose calculated to approximate human circulating TMAO levels [42],
219 followed 2 h, 6 h or 24 h later by assessment of Evans blue extravasation as described below.
220 Alternatively, mice were injected i.p. with 3 mg/kg body weight LPS or 100 µl 0.9% saline
221 vehicle, followed 2 h later by i.p. injection of either 1.8 mg/kg body weight TMAO or 100 µl
222 0.9% saline vehicle for assessment of Evans blue extravasation 2 h later. In both experiments,
223 one hour before assessment animals were injected i.p. with 100 µl of a 2 % (w/v) solution of
224 Evans blue dye in 0.9 % saline (Sigma–Aldrich Ltd, Poole, UK). Dye was permitted to circulate
225 for 1 h before animals were transcardially perfused with 0.9 % saline at 4 °C to remove
226 circulating dye. Brains were removed, bisected and homogenized by maceration in 0.9 %
227 saline. Suspended macromolecules were precipitated by incubation with 60 % trichloroacetic
228 acid, and dye content of resulting supernatants was detected using a CLARIOstar
229 spectrophotometer (BMG Labtech GmbH, Germany) alongside a standard curve of defined
230 concentrations of Evans blue in the same buffer. Brain Evans blue content was expressed as
231 µg of dye per mg of brain tissue, normalized to circulating plasma concentrations.
232
233 *Long-term LPS and TMAO treatments*
234 To assess the long-term impact of both LPS and TMAO on cognitive performance, mice were
235 divided into four groups (n=8 per group): 1) Water + PBS; 2) Water + TMAO; 3) LPS + PBS;
236 4) LPS + TMAO. C57Bl/6 mice were administered phosphate-buffered saline (PBS) or LPS
237 (*Escherichia coli* O55:B5, Sigma-Aldrich, UK) via i.p. injection (0.5 mg/kg/wk) for 8 weeks [43].
238 A final LPS treatment was administered the day before sacrifice for nine total injections. Body
239 weights were recorded prior to each injection. Starting on the day of the first saline/LPS
240 injection, TMAO was provided in the drinking water (500 mg/L), with water bottles being
241 replaced every other day. Drinking volumes were recorded before bottle change.
242
243 *Processing and analyses of RNAseq data*
244 Mice were transcardially perfused with 0.9 % saline at 4 °C to remove circulating blood, and
245 brains were removed and collected into RNAlater (Thermofisher Scientific Ltd., UK) prior to
246 storage at -20 °C for later analysis. Whole brain total RNA was extracted using a PureLink
247 RNA Mini Kit (Thermofisher Scientific Ltd., UK) and quantified using a CLARIOstar
248 spectrophotometer equipped with an LVis microplate (BMG Labtech GmbH, Germany). RNA

samples (*n*=3 TMAO, *n*=3 control) were sent to Macrogen Inc. (Republic of Korea) where they were subject to quality checks (RIN analysis); libraries were prepared (TruSeq Stranded mRNA LT Sample Prep Kit) for paired-end (2x 100 nt) sequencing on an Illumina HiSeq 4000 apparatus. Raw RNAseq sequence data (delivered in fastq format) were processed in house as follows. Reads were mapped onto the mouse genome (mm10) using HISAT2 v2.1.0 [44]. Number of reads in each sample that mapped to genes in the BAM files returned by HISAT2 was determined using featureCounts v1.6.4 [45]. Entrez gene identifiers were converted to gene symbols using *Mus musculus* annotations downloaded from NCBI on 26 November 2020; only those genes with valid Entrez gene identifiers were retained in analyses. Raw RNAseq data have been deposited with ArrayExpress under accession number E-MTAB-9869. Significantly differentially expressed genes ($P<0.1$) were analysed by mouse KEGG pathway over-representation analysis using Enrichr and manual curation.

Behavioural analyses

Behavioural tests were performed in the order they are introduced below. Apparatus was cleaned using 70 % ethanol upon completion of each trial, eliminating any residual odour.

Open field test (OFT) was conducted as previously described [46]. Briefly, mice were placed in the centre of the OFT, a grey 50 x 50 x 50 cm apparatus illuminated with low lux (100 lux) lighting. Total travel distance and time spent in the centre of the field was determined at 5 min with a video tracking system (Smart 3.0 tracking software, Panlab, Kent, UK).

The novel object recognition (NOR), a measure of recognition memory, was performed as described previously [47,48], with slight modifications. Briefly, on day 1 mice were habituated in a grey 50 x 50 x 50 cm apparatus illuminated with low lux (100 lux) lighting, mice were placed into the empty maze and allowed to move freely for 10 min. On day 2, mice were conditioned to a single object for a 10 min period. On day 3, mice were placed into the same experimental area in the presence of two identical objects for 15 min, after which they were returned to their respective cages and an inter-trial interval of 1 h was observed. One familiar object was replaced with a novel object, with the position of the novel object (left or right) being randomized between each mouse and group tested. Mice were placed back within the testing area for a final 10 min. Videos were analysed for a 5 min period, after which if an accumulative total of 15 s with both objects failed to be reached, analysis continued for the full 10 min or until 15 s was achieved. Those not achieving 15 s were excluded from the analysis [49]. A discrimination index (DI) was calculated as follows: $DI = (TN-TF)/(TN+TF)$, where TN is the time spent exploring the novel object and TF is the time spent exploring the familiar object.

286 Y-maze spontaneous alternation test, a measure of spatial working memory, was performed
287 on the final day of behavioural testing as previously described [50]. Briefly, the Y-maze
288 apparatus comprised white Plexiglas (dimensions 38.5 × 8 × 13 cm, spaced 120° apart) and
289 was illuminated with low lux (100 lux) lighting. Mice were placed in the maze and allowed to
290 explore freely for 7 min while tracking software recorded zone transitioning and locomotor
291 activity (Smart 3.0 tracking software, Panlab, Kent, UK). Spontaneous alternation was
292 calculated using the following formula: Spontaneous Alternation = (Number of alternations/
293 Total Arm entries - 2) x 100.
294
295 *Extravasation assay and sample processing following long-term treatment*
296 Twenty-four hours after the final injection of LPS, mice were injected i.p. with 200 µl of 2 %
297 sodium fluorescein in sterile ddH_2O and anesthetized 30 min later with isoflurane (1.5 %) in a
298 mixture of nitrous oxide (70 %), and oxygen (30 %). Once sedated, blood was collected by
299 cardiac puncture and centrifuged at 1,500 *g* for 15 min at 4 °C to collect the serum. The
300 samples were analysed immediately for sodium fluorescein extravasation or snap-frozen in
301 liquid nitrogen and stored at -80 °C until further analysis.
302
303 Mice were then transcardially perfused with saline containing 10 kU/ml heparin (Sigma,
304 Devon, UK). Dissected left hemi-brains were fixed in 4% PFA for 24 h and embedded into
305 paraffin before being processed for immunohistochemical analysis. Right hemi-brains were
306 stored at -80 °C until further analysis; cerebellums were processed immediately for the sodium
307 fluorescein extravasation assay. Cleared volume of sodium fluorescein that passed from the
308 plasma into the brain was calculated as described previously [43].
309
310 *Ex vivo immunohistochemical analysis*
311 Paraffin-embedded brains were sectioned (5 µm) using a rotary microtome and collected onto
312 glass microscope slides. Following deparaffinisation using xylene and rehydration using
313 graded ethanol:water solutions, heat-mediated antigen retrieval was performed by incubation
314 in 10 mM Tris base, 1 mM EDTA, 0.05 % Tween-20, pH 9.0 at 90 °C for 20 min. Once cooled,
315 endogenous peroxide activity was quenched by incubation for 15 min in 0.3 % H_2O_2 in Tris-
316 buffered saline (TBS; 50 mM Tris base, 150 mM NaCl, pH 7.4). Sections were permeabilised
317 and blocked by incubation in TBS containing 0.025% triton X-100 and 10 % normal goat serum
318 for 30 min, prior to overnight treatment at 4 °C with rabbit anti-murine primary antibodies raised
319 against GFAP (1:1000, ab7260, Abcam Ltd, UK) or Iba1 (1:1000, 019-19741, FUJIFILM Wako
320 Pure Chemical Corporation, Japan) diluted in TBS containing 1 % normal goat serum, 0.025
321 % Triton X-100, pH 7.4. Sections were washed thoroughly with TBS containing 1 % normal
322 goat serum and incubated for 1 h at room temperature with a horseradish peroxidase-

323 conjugated goat anti-rabbit antibody (1:500, Stratech Scientific, UK) diluted in TBS containing
324 1 % normal goat serum, 0.025 % Triton X-100, pH 7.4). Sections were thoroughly washed in
325 TBS and peroxidase staining was developed using diaminobenzidine hydrochloride and H_2O_2.
326 Sections were dehydrated with graded ethanol:water solutions, cleared with xylene and
327 mounted under DPX for microscopic examination. Brightfield images were captured using a
328 using a Nikon Eclipse 80i Stereology Microscope fitted with an Optronics Camera, using a 20x
329 objective, and analysed with ImageJ 1.53 k software (National Institutes of Health, USA).
330
331 *Statistical analyses*
332 Sample sizes were calculated to detect differences of 15 % or more with a power of 0.85 and
333 α set at 5 %, calculations being informed by previously published data [2,31]. *In vitro*
334 experimental data (except those for *in vitro* microarray experiments) are expressed as mean
335 ± SEM, with a minimum of $n = 3$ independent experiments performed in triplicate for all studies.
336 In all cases, normality of distribution was established using the Shapiro–Wilks test, followed
337 by analysis with two-tailed Student's *t*-tests to compare two groups or, for multiple comparison
338 analysis, 1- or 2-way ANOVA followed by Tukey's HSD *post hoc* test, or Dunnett's test for
339 dose-response experiments. Where data were not normally distributed, non-parametric
340 analysis was performed using the Wilcoxon signed rank test. A *P* value of less than or equal
341 to 5 % was considered significant. Differentially expressed genes were identified in microarray
342 data using LIMMA [51]; *P* values were corrected for multiple testing using the Benjamini–
343 Hochberg procedure (False Discovery Rate); a *P* value of less than or equal to 10 % was
344 considered significant in this case; $n = 5$ for control, TMAO and TMA groups. Significantly
345 differentially expressed genes ($P_{FDR}<0.1$) in RNAseq data (Supplementary Table 11) were
346 identified using DESeq2 v1.22.1 [52].
347

348 **RESULTS**

349 To provide an initial assessment of the effects of the methylamines TMA and TMAO upon the
350 BBB we used a well-established *in vitro* BBB model, hCMEC/D3 immortalised human
351 cerebromicrovascular cell monolayers grown under polarising conditions on a Transwell filter,
352 examining two key barrier properties: paracellular permeability to a protein-sized tracer and
353 TEER. Exposure of hCMEC/D3 cells for 24 h to TMA (0-40 μM) caused a clear dose-
354 dependent increase in paracellular permeability to 70 kDa FITC-dextran (Fig. 1A), with normal
355 circulating levels (0.4 μM) of TMA and upwards significantly enhancing permeability. In
356 contrast, exposure for 24 h to TMAO (0-4000 μM) caused a biphasic dose-dependent
357 response (Fig. 1A), with normal circulating concentrations (4-40 μM) significantly reducing
358 permeability to the tracer, an effect lost at 2.5-fold greater TMAO concentrations and reversed
359 at 100-fold greater TMAO (4 mM), where a significant increase in paracellular permeability
360 was apparent. In contrast, TMA had no effect upon TEER at any concentration studied, while
361 TMAO enhanced TEER by approximately 65%, an effect that was notably dose-independent
362 (Fig. 1B).
363
364 The physical barrier that the BBB provides is only one aspect by which it separates the brain
365 parenchymal environment from the periphery, equally important is the immunological barrier
366 that it represents. To model this, we employed a simple system in which adhesion of CMFDA-
367 labelled U937 monocytic cells to TNFα-activated (10 ng/ml, 16 h) hCMEC/D3 monolayers was
368 quantified in response to TMA or TMAO treatment. Treatment with a physiologically relevant
369 concentration of TMA (0.4 μM [42], 24 h post-TNFα) had no effect on the density of adherent
370 U937 cells, but exposure of hCMEC/D3 monolayers to physiological levels of TMAO (40 μM
371 [42], 24 h post-TNFα) significantly reduced U937 cell adhesion by approximately 50 %
372 compared to cultures stimulated with TNFα alone (Fig. 1C).
373
374 The endothelial cells of the BBB express numerous efflux transporter proteins that serve to
375 limit entry of endogenous and exogenous molecules into the parenchyma, with BCRP and P-
376 glycoprotein being two of the most important. Consequently, we examined whether treatment
377 with TMA or TMAO affected function or expression of either of these two transporters. Using
378 commercially available *in vitro* assays, neither methylamine affected BCRP nor P-glycoprotein
379 activity across a wide concentration range (TMA: 4.9 nM to 10.8 μM; TMAO 0.5 μM to 1.08
380 mM) (Suppl. Fig. 2A-D). Similarly, treatment of hCMEC/D3 cells for 24 h with physiologically
381 relevant concentrations of TMA (0.4 μM) or TMAO (40 μM) was without effect on cell surface
382 expression of either BCRP or P-glycoprotein (Suppl. Fig. 2E-F).
383

384 *Methylamine-induced changes in gene expression*
385 Having identified significant TMA-/TMAO-induced functional changes in endothelial barrier
386 characteristics *in vitro*, we undertook a microarray analysis of hCMEC/D3 cells treated with
387 either TMA (0.4 μM, 24 h) or TMAO (40 μM, 24 h) to investigate the transcriptional changes
388 underlying these effects. Treatment with TMA had a significant (P_{FDR}<0.1) effect on 49 genes,
389 with the expression of 39 upregulated and 10 downregulated (Fig 2A, Supplementary Table
390 2). In contrast, treatment with TMAO had a significant (P_{FDR}<0.1) effect on 440 genes with 341
391 upregulated and 99 downregulated (Fig. 2B, Supplementary Table 3). *FMO3* gene expression
392 was not affected by TMA or TMAO at the physiological concentrations employed (Suppl. Fig.
393 3).
394
395 SPIA of the 440 TMAO-affected genes showed activation of the tight junction pathway (P =
396 0.031), but significance was lost after correction for multiple testing (Supplementary Table 4).
397 No pathways were shown to be activated or inactivated by the 49 TMA-affected genes (data
398 not shown).
399
400 Gene ontology (GO) analysis was performed on TMA- and TMAO-regulated genes using
401 Enrichr [36,37]. TMA up-regulated and down-regulated genes were significantly (P_{FDR}<0.2)
402 associated with processes indicative of a degree of cellular stress (Fig 2C, Supplementary
403 Table 5, Supplementary Table 6). In contrast, genes up-regulated by TMAO treatment were
404 associated with regulation of the cytoskeleton and cell morphology and with actin bundle
405 formation (P_{FDR}<0.2), whereas pathways associated with inflammatory signalling were down-
406 regulated (Fig 2D, Supplementary Table 7, Supplementary Table 8).
407
408 We then assessed the topology of a directional network of the 440 TMAO-associated genes
409 mapped onto all human KEGG pathways. In line with the GO analysis described above, a
410 number of genes of differing function were regulated by TMAO treatment, with two principal
411 groupings being particularly evident, namely those associated with aspects of cellular
412 metabolism and with regulation of actin cytoskeletal dynamics (Figure 2E). Finally, we
413 compared the 19,309 genes represented on the microarray with a set of 203 genes [2] known
414 to be associated with the BBB. While TMA treatment had no significant effects on expression
415 of these genes (Supplementary Table 9), TMAO significantly (P_{FDR}<0.1) upregulated
416 expression of four genes from this set associated with transporter proteins and barrier integrity
417 (Table 1, Supplementary Table 10).
418
419 Given these transcriptional indications, and the fact that the restrictive properties of the BBB
420 are largely governed by inter-endothelial cell tight junctions linked *via* the zonula occludens

421 complex to the actin cytoskeleton [53], we hypothesised that TMA and TMAO may affect
422 barrier permeability through modification of the links between tight junctions and the actin
423 cytoskeleton. Confocal immunofluorescence microscopy of hCMEC/D3 monolayers treated
424 with a physiologically relevant concentration of TMA (0.4 μM, 24 h) or TMAO (40 μM, 24 h)
425 revealed clear changes to both ZO-1 and fibrillar actin disposition within cells (Fig. 2F).
426 Compared to untreated cells in which both ZO-1 and F-actin fibres clearly defined the cellular
427 perimeter, cells treated with TMA exhibited a broken, patchy distribution of perimeter ZO-1
428 expression, and the appearance of marked cytoplasmic F-actin stress fibres. In contrast, cells
429 treated with TMAO showed little change in ZO-1 distribution, but a marked enhancement of
430 cortical F-actin fibre thickness and intensity.
431
432 *The actions of TMAO are mediated through annexin A1 signalling*
433 Of the four BBB-associated genes identified as upregulated by TMAO, *ANXA1* is of particular
434 interest as we have previously shown this protein to regulate BBB tightness *in vitro* and *in vivo*
435 through modulation of the actin cytoskeleton [54]. Examination of ANXA1 expression in
436 hCMEC/D3 cells revealed that while total cellular levels of the protein were not changed by
437 either TMA (0.4 μM, 24 h) or TMAO (40 μM, 24 h) treatment (Fig. 3A), TMA significantly
438 suppressed and TMAO significantly augmented medium ANXA1 content (Fig. 3B), a finding
439 of interest given that autocrine/paracrine effects are a major route of ANXA1 action [55].
440
441 To establish the importance of ANXA1 in mediating the effects of TMAO, we investigated the
442 effects of its depletion through use of hCMEC/D3 clones stably transfected with shRNA
443 sequences targeting *ANXA1* mRNA (Suppl. Fig. 1). As we have reported previously [31],
444 suppression of *ANXA1* expression led to a baseline increase in paracellular permeability and
445 reduction in TEER. Notably, however, suppression of *ANXA1* expression significantly inhibited
446 the effects of TMAO (40 μM, 24 h) upon both paracellular permeability and TEER (Fig. 3C-D)
447 to a degree that correlated with extent of *ANXA1* suppression across different clones (57/61,
448 60A and 60B expressing approximately 20, 50 and ~70 % lower levels of annexin A1,
449 respectively), an effect not seen in cells bearing non-targeting scramble shRNA sequences.
450 The actions of ANXA1 are mediated to a large extent through the G protein-coupled receptor
451 formyl peptide receptor 2 (FPR2) [56]. Hence, we investigated how inclusion of a well-
452 characterised antagonist to this receptor, WRW_4 (10 μM, 10 min pre-treatment), would affect
453 the functional response to TMAO. Pre-treatment with WRW_4 was able to significantly attenuate
454 the effects of TMAO treatment on both TEER (Fig. 3E) and paracellular permeability (Fig. 3F),
455 further indicating the role of ANXA1 signalling as the principal mediator of TMAO actions on
456 hCMEC/D3 cells.
457

458 *Acute TMAO treatment enhances BBB integrity in vivo*
459 While hCMEC/D3 endothelial cells are a widely used and generally representative model, they
460 cannot reflect all aspects of the multicellular neurovascular unit that underlies BBB function,
461 hence we investigated whether the beneficial effects of TMAO identified *in vitro* translate to
462 an *in vivo* situation. Initial studies revealed that systemic administration of TMAO to wild-type
463 male mice (1.8 mg/kg, i.p.) induced a time-dependent reduction in BBB permeability to the
464 tracer Evans blue (2 % in saline, 100 µl, i.p.), with a significant reduction in dye extravasation
465 to the brain parenchyma being apparent 2 h following TMAO administration, an effect lost at
466 longer time-points (Fig. 4A), presumably due to the relatively short plasma half-life of TMAO
467 *in vivo* [5,57]. To further investigate this effect of TMAO, we employed a simple model of
468 enhanced BBB permeability, namely acute peripheral administration of bacterial LPS [31].
469 Treatment with LPS (*E. coli* O111:B4, 3 mg/kg, i.p.) significantly enhanced intraparenchymal
470 extravasation of Evans blue within 4 h, an effect significantly attenuated by subsequent
471 treatment with TMAO (1.8 mg/kg, i.p.) 2 h post-LPS (Fig. 4B), further confirming a beneficial
472 action of TMAO at physiological concentrations upon the BBB *in vivo*.
473
474 *TMAO treatment rapidly alters brain transcriptional activity*
475 To investigate the wider actions of TMAO upon the brain we performed whole brain RNAseq
476 transcriptomic analysis of wild-type male mice 2 h following TMAO administration (1.8 mg/kg
477 i.p.). We identified 76 significantly differentially expressed genes (P_{FDR}<0.1), with expression
478 of 41 upregulated and 35 downregulated (Figure 5A; Supplementary Table 11). KEGG
479 pathway analysis using Enrichr identified a number of significantly regulated murine pathways
480 (Figure 5B), including oxidative phosphorylation, Parkinson's disease and Alzheimer's
481 disease. Closer analysis of regulated genes identified several general groupings (Figure 5C),
482 with downregulated genes associated with the mitochondrial respiratory chain (*COX1*, *COX3*,
483 *ATP6*, *ND4L*, *CYTB*, *ND1*, *ND3*, *ND4*, *ND6*) and ribosomal function (*mt-Rnr2*, *mt-Rnr1*,
484 *Rps23rg1*) and upregulated genes associated with cellular or axonal growth (*Nme7*, *B3gat2*,
485 *Fuz*, *Nefm*, *Basp1*, *Mtg1*, *Vps37a*, *Smim1*, *Araf*). Of the 203 BBB-associated human genes
486 previously identified [2], 197 had matches in our mouse brain data set. Here, two genes were
487 identified as significantly differentially expressed at P_{FDR}<0.1: reduced *Cpe* (carboxypeptidase
488 E) and increased *App* (amyloid precursor protein) expression (Figure 5D; Supplementary
489 Table 12).
490
491 *Chronic low-dose TMAO treatment prevents LPS-induced BBB disruption and memory*
492 *impairment*
493 The fundamental role of the BBB is to protect the brain and preserve its homeostatic
494 environment; damage to BBB integrity is therefore detrimental, and is believed to directly

495 contribute towards cognitive impairment [58]. Having shown TMAO to exert a beneficial effect
496 upon BBB function/integrity in response to acute inflammatory insult, we next examined
497 whether a similar effect held true for chronic conditions, and whether any protection extended
498 to cognition. TMAO was administered to male C57Bl/6J mice through drinking water (0.5
499 mg/ml) over 2 months, in combination with chronic low-dose LPS administration (0.5
500 mg/kg/week, i.p.) to model a mild inflammatory stress known to impact cognitive behaviour
501 [43]. There were no differences in volumes of water drunk or, where relevant, final
502 consumption of TMAO between any groups (Table 2). The serum inflammatory cytokines
503 TNFα and IL-1β were both nominally elevated in response to LPS treatment, although not
504 reaching statistical significance, indicating a sub-clinical inflammatory response; TMAO had
505 no effect on TNFα nor IL-1β levels (Suppl. Fig. 4). Notably, animals exposed to LPS exhibited
506 a significant reduction in body weight gain compared to their untreated counterparts, an effect
507 reversed by TMAO treatment (Fig. 6A). Treatment with LPS increased cerebellar FITC
508 extravasation, an effect that was prevented by TMAO treatment, although this did not reach
509 statistical significance on *post hoc* analysis (Fig. 6B). To corroborate these findings, we
510 investigated a second marker of impaired BBB integrity, confocal microscopic detection of
511 brain perivascular IgG deposition. In comparison with sham-treated animals, exposure to LPS
512 caused a significant accumulation of IgG in the perivascular compartment, an effect prevented
513 by TMAO treatment (Fig. 6C).
514
515 The OFT confirmed neither LPS nor TMAO treatment affected motor function, with movement
516 speed and distance travelled comparable across treatment groups (Fig. 6D-E). Similarly, no
517 effect was apparent on the proportion of time animals spent in the centre of the field,
518 suggesting limited effects upon anxiety (Fig. 6F). Working memory, however, determined via
519 NOR indicated a significant reduction in performance in animals exposed to LPS, a
520 behavioural deficit notably prevented in animals co-treated with TMAO (Fig. 6G). In contrast,
521 no effect of either LPS or TMAO treatment was apparent in the Y-maze spontaneous
522 alternation task (Fig. 6H) or in distance travelled during this task (Fig. 6I), indicating no
523 differences in spatial memory.
524
525 The brain circuitry thought to underlie spatial and recognition memory functions are known to
526 differ, with greater relative involvement of the hippocampus and
527 entorhinal/perirhinal/retrosplenial cortices, respectively [59,60]. As the underlying cognitive
528 lesion in the NOR task was induced by LPS, we investigated the impact of LPS or TMAO
529 treatment on principal inflammation-responsive CNS cells, astrocytes and microglia, in the
530 entorhinal cortex and hippocampus. Exposure to LPS caused a significant reduction in primary

531 process number for both GFAP+ astrocytes and Iba1+ microglia in the entorhinal cortex,
532 changes that were effectively prevented by TMAO treatment (Fig. 7A-C). Notably, however,
533 no differences were seen in either astrocyte or microglial morphology in the neighbouring
534 hippocampus (Fig. 7E-G); no differences were apparent in either astrocyte or microglial
535 density in either region (Fig. 7D, H).
536

537 **DISCUSSION**

538

539 The relationship between the BBB and cognitive behaviour is complex and far from being fully
540 understood, but it is clear from both human and animal studies that deficits in barrier integrity
541 can exert a profound and deleterious effect upon memory, language and executive function
542 [61–64]. Indeed, BBB impairment is among the first events to occur in the course of
543 Alzheimer's disease, and may aggravate the pathological processes that underlie the
544 condition [65]. Strategies to promote BBB function may thus have significant value in helping
545 to protect the brain from progressive neurological diseases such as dementia. In this study we
546 identify novel and distinct roles for the microbiome-associated dietary methylamines TMA and
547 TMAO in regulating BBB function *in vitro* and *in vivo* and provide evidence that the beneficial
548 action of TMAO upon the BBB under inflammatory conditions coincides with similarly positive
549 effects upon glial activity and cognition. These data reinforce the position of the cerebral
550 vasculature as a major target for the gut-brain axis, and extend our knowledge of its
551 interactions with microbial metabolites beyond SCFAs [1,2] to another major class of
552 molecules, the dietary methylamines.

553

554 Notably, our data show that while both TMA and TMAO have activity upon the endothelium,
555 there is a marked distinction between their effects despite their close structural similarity. TMA,
556 a volatile organic compound and the direct product of microbial choline, L-carnitine and TMAO
557 metabolism in the upper gut [5], had a deleterious effect upon the endothelium, disrupting
558 cytoskeletal arrangement, inducing signs of metabolic stress and ultimately impairing
559 endothelial barrier integrity. In contrast, TMAO, an inert small molecule largely derived from
560 hepatic FMO3-mediated oxidation of TMA taken up from the gut via the hepatic portal vein [6],
561 promoted cerebral vascular integrity *in vitro* and *in vivo*. These differences suggest that host
562 conversion of TMA (a gas) to TMAO (a stable metabolite) may be an effective detoxification
563 pathway, emphasising the importance of host metabolic pathways in modulating
564 communication in the gut-brain axis, and underlining the importance of using a systems-level
565 approach to understand the interactions between the host and its resident microbiota.

566

567 The primary focus of this work was on the effects of TMAO upon the BBB, but this is not
568 necessarily the only CNS target for the methylamine. Our data add to the evidence suggesting
569 that astrocytes [66,67] and microglia [68,69] may respond to TMAO treatment, although it is
570 notable that previous studies have shown pro-activating effects of TMAO at supra-
571 physiological concentrations (>50 μM). An intriguing finding of the current study is the brain
572 region selectivity in the effects of long-term LPS and/or TMAO treatment upon parenchymal
573 glia, with astrocytes and microglia of the entorhinal cortex showing clear LPS-induced, TMAO-

574 sensitive activation, whereas the same cell types in the neighbouring hippocampus appeared
575 resistant to either stimulus. Notably, this closely accords with the involvement of these areas
576 in recognition and spatial memory tasks [59,60], potentially underpinning the cognitive
577 consequences of LPS and TMAO treatment. Determining why this regional discrepancy
578 occurs lies outside the scope of the present study, but it may be relevant that differences have
579 been identified in both neurovascular unit microanatomy [70] and in vascular density [71]
580 between the hippocampus and cortical areas. Ultimately, interpretation of the cell-type-specific
581 responses to TMAO treatment and their interactions with each other, particularly in the context
582 of understanding cognitive implications, will require use of more sensitive analytical
583 techniques such as single-cell transcriptomics, but this remains a fascinating avenue for future
584 study.
585
586 Numerous groups have investigated the putative relationship between TMAO and cognition
587 following reports of an association between cerebrospinal fluid TMAO content and Alzheimer's
588 disease [28], with negative correlations between plasma TMAO content and cognitive function
589 having been identified in both clinical [66,72,73] and experimental [29,68,69] settings. Whether
590 this relationship is truly deterministic remains unclear, however, as the role of the immediate
591 precursor to TMAO – TMA – in cognition and vascular function has largely been overlooked.
592 This omission may be important in light of studies reporting negative correlations between
593 cognitive impairment and serum TMA [74–76] and our own data showing a potent detrimental
594 effect of physiological levels of TMA upon the cerebrovascular endothelium *in vitro*. Given that
595 TMA has also been shown to be detrimental in contexts other than cognitive function [22,23],
596 the contribution that this metabolite plays in disease is evidently in need of closer attention.
597
598 Interpreting associations between circulating TMAO and cognition is further complicated by
599 studies indicating that consumption of the TMAO precursors choline and L-carnitine can
600 improve cognitive function [24,25,77], evidence that patients with Parkinson's disease have
601 lower circulating TMAO than healthy controls [78], and more-recent Mendelian randomisation
602 analysis indicating that serum TMAO and Alzheimer's disease are not causally related [79].
603 Given this background, our data indicating that physiologically relevant concentrations of
604 TMAO have positive effects upon both BBB integrity and cognition *in vivo* thus serve as a
605 useful counterweight to population-level correlation studies. Interestingly, a number of
606 previous interventional studies have been performed in mice, suggesting that substantially
607 higher doses of TMAO may have detrimental effects upon learning and memory [68,69,80],
608 although as we and others [81] have identified dose-dependency in the effects of TMAO *in*
609 *vitro*, it seems plausible that this may reflect a similar phenomenon *in vivo*. The importance of
610 investigating the impact of TMAO under physiologically relevant conditions is further

611 emphasised by a recent study showing TMAO treatment to impair novel object recognition in
612 mice [66], ostensibly an opposite finding to our data achieved with a similar dosing regimen.
613 Importantly, however, mice in this study were maintained on a reduced choline diet, a condition
614 known to alter hepatic metabolism [82]; what impact such changes might have on handling of
615 (TMA and) TMAO by the body is unknown. These discrepancies may be instructive in guarding
616 against incautious extrapolation of TMAO effects from healthy to diseased populations.
617
618 Consumption of a diet rich in fish and other seafood, known to provide significant quantities of
619 TMAO [83], associates with a reduced risk of cognitive decline [84,85] and protection against
620 cerebrovascular disease [86]. These effects have in large part been attributed to beneficial
621 actions of the omega-3 polyunsaturated fatty acids [87], although there is little evidence that
622 their direct supplementation improves cognitive function [88] or stroke risk [89]. Here we
623 provide evidence that another component of a seafood-rich diet, TMAO, has protective effects
624 on the cerebral vasculature, astrocyte and microglial function, and upon cognition. Moreover,
625 fish consumption has been associated with reduced inflammatory disease, again attributed
626 primarily to a role for omega-3 fatty acids [90]. While it is too early to definitively claim an anti-
627 inflammatory role for dietary methylamines, particularly given the opposing actions of TMA
628 and TMAO, our data do indicate that broadening the scope of nutritional analyses of seafood-
629 rich diets beyond the omega-3 fatty acids may be worthwhile.
630
631 The data we report here indicate a clear reparative effect of TMAO upon BBB integrity
632 following acute inflammatory insult, and further suggest that long-term TMAO treatment may
633 be genuinely protective against prolonged sub-acute inflammatory challenge. Understanding
634 the mechanism(s) underlying these effects is complex, however, as LPS is known to impair
635 BBB function both directly at the endothelium [91] and following systemic cytokine induction
636 [92]. As TMAO acts via induction of ANXA1 release and ANXA1 is known both to enhance
637 BBB integrity [54] and to exert powerful pro-resolving actions at inflammatory foci [93],
638 either/both of these actions of LPS could conceivably be modulated by TMAO treatment.
639 Future studies giving TMAO in advance of BBB challenge may thus be necessary to fully
640 interpret its actions in human clinical settings.

641 **CONCLUSIONS**

642 Interest in the role played by the gut microbiota in communication through the gut-brain axis
643 has grown dramatically in the last few years, with much attention focused on the mediating
644 actions of microbe-derived metabolites [94]. While a number of studies have shown patterns
645 in microbial metabolite production that associate with different brain functions [95], detailed
646 understanding of the role of individual molecules remains in its infancy, with defined roles
647 characterised for only a subset of the many molecules known to be released by gut microbes.
648 Here we show that the dietary methylamine TMAO can beneficially modulate both BBB
649 integrity and cognitive function *in vivo*, providing direct mechanistic evidence for a positive role
650 of this microbiome-associated metabolite, and reinforce the position of the BBB as an interface
651 in the gut-brain axis. Notably, the positive effects of TMAO that we report stand in contrast to
652 previous work describing deleterious effects of TMAO exposure at high concentrations or
653 under non-physiological conditions [81], emphasising the importance of taking a holistic
654 approach to understanding gut microbiota-host interactions.

655 **LIST OF ABBREVIATIONS**

656 BBB, blood–brain barrier; DI, discrimination index; GO, gene ontology; KEGG, Kyoto
657 Encyclopedia of Genes and Genomes; LPS, lipopolysaccharide; NOR, novel object
658 recognition; SCFA, short-chain fatty acid; OFT, open field test; SPIA, signalling pathway
659 impact analysis; TEER, transendothelial electrical resistance; TMA, trimethylamine; TMAO,
660 trimethylamine *N*-oxide.

661

662 **DECLARATIONS**

663

664 ***Ethics approval and consent to participate***

665 Not applicable

666

667 ***Consent for publication***

668 Not applicable

669

670 ***Availability of data and materials***

671 Cell line array data have been deposited in ArrayExpress under accession number E-MTAB-
672 6662. Raw murine RNAseq data have been deposited with ArrayExpress under accession
673 number E-MTAB-9869. Supplementary materials associated with the article are available from
674 figshare (https://doi.org/10.6084/m9.figshare.13549334.v1).

675

676 ***Competing interests***

677 The authors declare that they have no competing interests.

678

679 ***Funding***

680 This work was funded by Alzheimer's Research UK Pilot Grant No. ARUK-PPG2016B-6.
681 PREDEASY™ efflux transporter analysis kits were generously provided through the SOLVO
682 Biotechnology Research and Academic Collaborative Transporter Studies (ReACTS)
683 Program. This work used the computing resources of the UK MEDical BIOinformatics
684 partnership – aggregation, integration, visualisation and analysis of large, complex data (UK
685 MED-BIO), which was supported by the Medical Research Council (grant number
686 MR/L01632X/1). SF was supported by Fundación Alfonso Martín Escudero. TS was supported
687 by a bursary from the Imperial College London Undergraduate Research Opportunities
688 Programme.

689

690 ***Author contributions***

691 LH, DV and SM designed the experiments. SM performed cellular assays and acute *in vivo*/*ex*
692 *vivo* analyses. TS carried out the initial permeability and TEER assays. KSJ performed glial
693 immunohistochemical analyses. MAA performed IgG extravasation studies. ES produced and
694 provided shRNA treated hCMEC/D3 clones. LH undertook all processing and analyses of
695 transcriptomic data. RCG provided valuable insight and advice throughout the project. DV,
696 MP, IR and MM performed the chronic *in vivo* LPS challenge study and undertook all analyses
697 of behavioural data. SRC, ALC and SF contributed to preliminary animal work. LH, DV and
698 SM wrote the manuscript. All authors read and approved the final version of the manuscript.
699

700 ***Acknowledgements***
701 Not applicable
702

703 **REFERENCES**

704 1. Braniste V, Al-Asmakh M, Kowal C, Anuar F, Abbaspour A, Tóth M, et al. The gut microbiota
705 influences blood-brain barrier permeability in mice. Sci Transl Med. 2014;6:263ra158.

706 2. Hoyles L, Snelling T, Umlai U-K, Nicholson JK, Carding SR, Glen RC, et al. Microbiome–
707 host systems interactions: protective effects of propionate upon the blood–brain barrier.
708 Microbiome. 2018;6:55–55.

709 3. Tang WHW, Hazen SL. Microbiome, trimethylamine N-oxide, and cardiometabolic disease.
710 Transl Res. 2017;179:108–15.

711 4. Dinicolantonio JJ, McCarty M, Okeefe J. Association of moderately elevated trimethylamine
712 N-oxide with cardiovascular risk: Is TMAO serving as a marker for hepatic insulin resistance.
713 Open Heart. 2019;6:e000890–e000890.

714 5. Hoyles L, Jimenez-Pranteda ML, Chilloux J, Brial F, Myridakis A, Aranias T, et al. Metabolic
715 retroconversion of trimethylamine N-oxide and the gut microbiota. Microbiome. 2018;6:73–73.

716 6. Zeisel SH, Wishnok JS, Blusztajn JK. Formation of methylamines from ingested choline
717 and lecithin. J Pharmacol Exp Ther. United States; 1983;225:320–4.

718 7. Kühn T, Rohrmann S, Sookthai D, Johnson T, Katzke V, Kaaks R, et al. Intra-individual
719 variation of plasma trimethylamine-N-oxide (TMAO), betaine and choline over 1 year. Clin
720 Chem Lab Med. 2017;55:261–8.

721 8. Duranton F, Cohen G, De Smet R, Rodriguez M, Jankowski J, Vanholder R, et al. Normal
722 and pathologic concentrations of uremic toxins. J Am Soc Nephrol. 2012;23:1258–70.

723 9. Bain M, Faull R, Fornasini G, Milne R, Evans A. Accumulation of Trimethylamine and
724 trimethylamine-N-oxide in End-Stage Renal Disease Patients Undergoing Haemodialysis.
725 Nephrol Dial Transplant. 2006;21:1300–4.

726 10. Tang WHW, Wang Z, Levison BS, Koeth RA, Britt EB, Fu X, et al. Intestinal microbial
727 metabolism of phosphatidylcholine and cardiovascular risk. N Engl J Med. 2013;368:1575–84.

728 11. Tang WHW, Wang Z, Fan Y, Levison B, Hazen JE, Donahue LM, et al. Prognostic value
729 of elevated levels of intestinal microbe-generated metabolite trimethylamine-N-oxide in
730 patients with heart failure: refining the gut hypothesis. J Am Coll Cardiol. 2014;64:1908–14.

731 12. Wang Z, Roberts AB, Buffa JA, Levison BS, Zhu W, Org E, et al. Non-lethal Inhibition of
732 Gut Microbial Trimethylamine Production for the Treatment of Atherosclerosis. Cell.
733 2015;163:1585–95.

734 13. Zhu W, Gregory JC, Org E, Buffa JA, Gupta N, Wang Z, et al. Gut Microbial Metabolite
735 TMAO Enhances Platelet Hyperreactivity and Thrombosis Risk. Cell. 2016;165:111–24.

736 14. Aldana-Hernández P, Leonard K-A, Zhao Y-Y, Curtis JM, Field CJ, Jacobs RL. Dietary
737 Choline or Trimethylamine N-oxide Supplementation Does Not Influence Atherosclerosis
738 Development in Ldlr−/− and Apoe−/− Male Mice. J Nutr. 2019;

739 15. Miller CA, Corbin KD, da Costa K-A, Zhang S, Zhao X, Galanko JA, et al. Effect of egg
740 ingestion on trimethylamine-N-oxide production in humans: a randomized, controlled, dose-
741 response study. Am J Clin Nutr. 2014;100:778–86.

742 16. Jia J, Dou P, Gao M, Kong X, Li C, Liu Z, et al. Assessment of Causal Direction Between
743 Gut Microbiota-Dependent Metabolites and Cardiometabolic Health: Abi-Directional
744 Mendelian Randomisation Analysis. Diabetes. 2019;68:1747–55.

745 17. Winther SA, Ollgaard JC, Tofte N, Tarnow L, Wang Z, Ahluwalia TS, et al. Utility of Plasma
746 Concentration of Trimethylamine N-Oxide in Predicting Cardiovascular and Renal
747 Complications in Individuals With Type 1 Diabetes. Diabetes Care. 2019;42:1512–20.

748 18. Huc T, Drapala A, Gawrys M, Konop M, Bielinska K, Zaorska E, et al. Chronic, low-dose
749 TMAO treatment reduces diastolic dysfunction and heart fibrosis in hypertensive rats. Am J
750 Physiol. 2018;315:H1805–20.

751 19. Collins HL, Drazul-Schrader D, Sulpizio AC, Koster PD, Williamson Y, Adelman SJ, et al.
752 L-Carnitine intake and high trimethylamine N-oxide plasma levels correlate with low aortic
753 lesions in ApoE−/− transgenic mice expressing CETP. Atherosclerosis. 2016;244:29–37.

754 20. Zhao Z-H, Xin F-Z, Zhou D, Xue Y-Q, Liu X-L, Yang R-X, et al. Trimethylamine N-oxide
755 attenuates high-fat high-cholesterol diet-induced steatohepatitis by reducing hepatic
756 cholesterol overload in rats. World J Gastroenterol. 2019;25:2450–62.

757 21. Dumas M-E, Rothwell AR, Hoyles L, Aranias T, Chilloux J, Calderari S, et al. Microbial-
758 Host Co-metabolites Are Prodromal Markers Predicting Phenotypic Heterogeneity in Behavior,
759 Obesity, and Impaired Glucose Tolerance. Cell Rep. 2017;20:136–48.

760 22. Jaworska K, Bielinska K, Gawrys-Kopczynska M, Ufnal M. TMA (trimethylamine), but not
761 its oxide TMAO (trimethylamine-oxide), exerts haemodynamic effects: implications for
762 interpretation of cardiovascular actions of gut microbiome. Cardiovasc Res. 2019;115:1948–
763 9.

764 23. Huo X, Li J, Cao Y-F, Li S-N, Shao P, Leng J, et al. Trimethylamine N-Oxide Metabolites
765 in Early Pregnancy and Risk of Gestational Diabetes: A Nested Case-Control Study. J Clin
766 Endocrinol Metab. 2019;104:5529–39.

767 24. Poly C, Massaro JM, Seshadri S, Wolf PA, Cho E, Krall E, et al. The relation of dietary
768 choline to cognitive performance and white-matter hyperintensity in the Framingham Offspring
769 Cohort. Am J Clin Nutr. 2011;94:1584–91.

770 25. Nurk E, Refsum H, Bjelland I, Drevon CA, Tell GS, Ueland PM, et al. Plasma free choline,
771 betaine and cognitive performance: the Hordaland Health Study. Br J Nutr. 2013;109:511–9.

772 26. Leathwood PD, Heck E, Mauron J. Phosphatidyl choline and avoidance performance in
773 17 month-old SEC/1ReJ mice. Life Sci. 1982;30:1065–71.

774 27. Bartus RT, Dean RL, Goas JA, Lippa AS. Age-related changes in passive avoidance
775 retention: modulation with dietary choline. Science. 1980;209:301–3.

776 28. Vogt NM, Romano KA, Darst BF, Engelman CD, Johnson SC, Carlsson CM, et al. The gut
777 microbiota-derived metabolite trimethylamine N-oxide is elevated in Alzheimer's disease.
778 Alzheimers Res Ther. 2018;10:124–124.

779 29. Gao Q, Wang Y, Wang X, Fu S, Zhang X, Wang RT, et al. Decreased levels of circulating
780 trimethylamine N-oxide alleviate cognitive and pathological deterioration in transgenic mice:
781 A potential therapeutic approach for Alzheimer's disease. Aging. 2019;11:8642–63.

782 30. Weksler BB, Subileau EA, Perrière N, Charneau P, Holloway K, Leveque M, et al. Blood-
783 brain barrier-specific properties of a human adult brain endothelial cell line. FASEB J.
784 2005;19:1872–4.

785 31. Maggioli E, McArthur S, Mauro C, Kieswich J, Kusters DHM, Reutelingsperger CPM, et al.
786 Estrogen protects the blood-brain barrier from inflammation-induced disruption and increased
787 lymphocyte trafficking. Brain Behav Immun. 2015;51:212–22.

788 32. Abbott NJ, Hughes CC, Revest PA, Greenwood J. Development and characterisation of a
789 rat brain capillary endothelial culture: towards an in vitro blood-brain barrier. J Cell Sci.
790 1992;103 (Pt 1:23–37.

791 33. Coisne C, Dehouck L, Faveeuw C, Delplace Y, Miller F, Landry C, et al. Mouse syngenic
792 in vitro blood-brain barrier model: a new tool to examine inflammatory events in cerebral
793 endothelium. Lab Investig J Tech Methods Pathol. 2005;85:734–46.

794 34. Pais de Barros J-P, Gautier T, Sali W, Adrie C, Choubley H, Charron E, et al. Quantitative
795 lipopolysaccharide analysis using HPLC/MS/MS and its combination with the limulus
796 amebocyte lysate assay. J Lipid Res. 2015;56:1363–9.

797 35. Gautier L, Cope L, Bolstad BM, Irizarry RA. affy--analysis of Affymetrix GeneChip data at
798 the probe level. Bioinforma 2004;20:307–15.

799 36. Chen EY, Tan CM, Kou Y, Duan Q, Wang Z, Meirelles GV, et al. Enrichr: interactive and
800 collaborative HTML5 gene list enrichment analysis tool. BMC Bioinformatics. 2013;14:128–
801 128.

802 37. Kuleshov MV, Jones MR, Rouillard AD, Fernandez NF, Duan Q, Wang Z, et al. Enrichr: a
803 comprehensive gene set enrichment analysis web server 2016 update. Nucleic Acids Res.
804 2016;44:W90-7.

805 38. Tarca AL, Draghici S, Khatri P, Hassan SS, Mittal P, Kim J-S, et al. A novel signaling
806 pathway impact analysis. Bioinforma. 2009;25:75–82.

807 39. Hoyles L, Fernández-Real J-M, Federici M, Serino M, Abbott J, Charpentier J, et al.
808 Molecular phenomics and metagenomics of hepatic steatosis in non-diabetic obese women.
809 Nat Med. 2018;24:1070–80.

810 40. Zhang JD, Wiemann S. KEGGgraph: a graph approach to KEGG PATHWAY in R and
811 bioconductor. Bioinforma. 2009;25:1470–1.

812 41. McArthur S, Cristante E, Paterno M, Christian H, Roncaroli F, Gillies GEE, et al. Annexin
813 A1: a central player in the anti-inflammatory and neuroprotective role of microglia. J Immunol.
814 2010;185:6317–28.

815 42. Wishart DS, Feunang YD, Marcu A, Guo AC, Liang K, Vázquez-Fresno R, et al. HMDB
816 4.0: the human metabolome database for 2018. Nucleic Acids Res. 2018;46:D608–17.

817 43. Marottoli FM, Katsumata Y, Koster KP, Thomas R, Fardo DW, Tai LM. Peripheral
818 Inflammation, Apolipoprotein E4, and Amyloid-β Interact to Induce Cognitive and
819 Cerebrovascular Dysfunction: ASN Neuro. 2017;9:1759091417719201.

820 44. Kim D, Langmead B, Salzberg SL. HISAT: a fast spliced aligner with low memory
821 requirements. Nat Methods. 2015;12:357–60.

822 45. Liao Y, Smyth GK, Shi W. featureCounts: an efficient general purpose program for
823 assigning sequence reads to genomic features. Bioinforma 2014;30:923–30.

824 46. Hölter SM, Einicke J, Sperling B, Zimprich A, Garrett L, Fuchs H, et al. Tests for Anxiety-
825 Related Behavior in Mice. Curr Protoc Mouse Biol. 2015;5:291–309.

826 47. Davis KE, Eacott MJ, Easton A, Gigg J. Episodic-like memory is sensitive to both
827 Alzheimer's-like pathological accumulation and normal ageing processes in mice. Behav Brain
828 Res. 2013;254:73–82.

829 48. Leger M, Quiedeville A, Bouet V, Haelewyn B, Boulouard M, Schumann-Bard P, et al.
830 Object recognition test in mice. Nat Protoc. 2013;8:2531–7.

831 49. Denninger JK, Smith BM, Kirby ED. Novel Object Recognition and Object Location
832 Behavioral Testing in Mice on a Budget. J Vis Exp 2018;

833 50. Thomas R, Morris AWJ, Tai LM. Epidermal growth factor prevents APOE4-induced
834 cognitive and cerebrovascular deficits in female mice. Heliyon. 2017;3:e00319.

835 51. Ritchie ME, Phipson B, Wu D, Hu Y, Law CW, Shi W, et al. limma powers differential
836 expression analyses for RNA-sequencing and microarray studies. Nucleic Acids Res.
837 2015;43:e47–e47.

838 52. Love MI, Huber W, Anders S. Moderated estimation of fold change and dispersion for
839 RNA-seq data with DESeq2. Genome Biol. 2014;15:550.

840 53. Lochhead JJ, Yang J, Ronaldson PT, Davis TP. Structure, Function, and Regulation of the
841 Blood-Brain Barrier Tight Junction in Central Nervous System Disorders. Front Physiol.
842 2020;11:914.

843 54. Cristante E, McArthur S, Mauro C, Maggioli E, Romero IAIA, Wylezinska-Arridge M, et al.
844 Identification of an essential endogenous regulator of blood-brain barrier integrity, and its
845 pathological and therapeutic implications. Proc Natl Acad Sci U S A. 110:832–41.

846 55. McArthur S, Yazid S, Christian H, Sirha R, Flower R, Buckingham J, et al. Annexin A1
847 regulates hormone exocytosis through a mechanism involving actin reorganization. FASEB J.
848 2009;23:4000–10.

849 56. Bena S, Brancaleone V, Wang JM, Perretti M, Flower RJ. Annexin A1 interaction with the
850 FPR2/ALX receptor: identification of distinct domains and downstream associated signaling.
851 J Biol Chem. 2012;287:24690–7.

852 57. Cho CE, Taesuwan S, Malysheva OV, Bender E, Tulchinsky NF, Yan J, et al.
853 Trimethylamine-N-oxide (TMAO) response to animal source foods varies among healthy
854 young men and is influenced by their gut microbiota composition: A randomized controlled
855 trial. Mol Nutr Food Res. 2017;61:1600324.

856 58. Trigiani LJ, Bourourou M, Lacalle-Aurioles M, Lecrux C, Hynes A, Spring S, et al. A
857 functional cerebral endothelium is necessary to protect against cognitive decline. J Cereb
858 Blood Flow Metab 2021;271678X211045438.

859 59. Cohen SJ, Stackman RW. Assessing rodent hippocampal involvement in the novel object
860 recognition task. A review. Behav Brain Res. 2015;285:105–17.

861 60. Wilson DIG, Langston RF, Schlesiger MI, Wagner M, Watanabe S, Ainge JA. Lateral
862 entorhinal cortex is critical for novel object-context recognition. Hippocampus. 2013;23:352–
863 66.

864 61. Merino JG, Latour LL, Tso A, Lee KY, Kang DW, Davis LA, et al. Blood-brain barrier
865 disruption after cardiac surgery. Am J Neuroradiol. 2013;34:518–23.

866 62. Hu N, Guo D, Wang H, Xie K, Wang C, Li Y, et al. Involvement of the blood-brain barrier
867 opening in cognitive decline in aged rats following orthopedic surgery and high concentration
868 of sevoflurane inhalation. Brain Res. 2014;1551:13–24.

869 63. Abrahamov D, Levran O, Naparstek S, Refaeli Y, Kaptson S, Abu Salah M, et al. Blood-
870 Brain Barrier Disruption After Cardiopulmonary Bypass: Diagnosis and Correlation to
871 Cognition. Ann Thorac Surg. 2017;104:161–9.

872 64. Yang S, Gu C, Mandeville ET, Dong Y, Esposito E, Zhang Y, et al. Anesthesia and Surgery
873 Impair Blood-Brain Barrier and Cognitive Function in Mice. Front Immunol. 2017;8:902–902.

874 65. Zenaro E, Piacentino G, Constantin G. The blood-brain barrier in Alzheimer's disease.
875 Neurobiol Dis. 2016;107:41–56.

876 66. Brunt VE, LaRocca TJ, Bazzoni AE, Sapinsley ZJ, Miyamoto-Ditmon J, Gioscia-Ryan RA,
877 et al. The gut microbiome-derived metabolite trimethylamine N-oxide modulates
878 neuroinflammation and cognitive function with aging. GeroScience. 2021;43:377–94.

879 67. Su H, Fan S, Zhang L, Qi H. TMAO Aggregates Neurological Damage Following Ischemic
880 Stroke by Promoting Reactive Astrocytosis and Glial Scar Formation via the Smurf2/ALK5
881 Axis. Front Cell Neurosci. 2021;15:569424.

882 68. Zhao L, Zhang C, Cao G, Dong X, Li D, Jiang L. Higher Circulating Trimethylamine N-
883 oxide Sensitizes Sevoflurane-Induced Cognitive Dysfunction in Aged Rats Probably by
884 Downregulating Hippocampal Methionine Sulfoxide Reductase A. Neurochem Res.
885 2019;44:2506–16.

886 69. Meng F, Li N, Li D, Song B, Li L. The presence of elevated circulating trimethylamine N-
887 oxide exaggerates postoperative cognitive dysfunction in aged rats. Behav Brain Res.
888 2019;368:111902–111902.

889 70. Frías-Anaya E, Gromnicova R, Kraev I, Rogachevsky V, Male DK, Crea F, et al. Age-
890 related ultrastructural neurovascular changes in the female mouse cortex and hippocampus.
891 Neurobiol Aging. 2021;101:273–84.

892 71. Schaffenrath J, Huang S-F, Wyss T, Delorenzi M, Keller A. Characterization of the blood-
893 brain barrier in genetically diverse laboratory mouse strains. Fluids Barriers CNS. 2021;18:34.

894 72. He W, Luo Y, Liu J-P, Sun N, Guo D, Cui L-L, et al. Trimethylamine N-Oxide, a Gut
895 Microbiota-Dependent Metabolite, is Associated with Frailty in Older Adults with
896 Cardiovascular Disease. Clin Interv Aging. 2020;15:1809–20.

897 73. Zhu C, Li G, Lv Z, Li J, Wang X, Kang J, et al. Association of plasma trimethylamine-N-
898 oxide levels with post-stroke cognitive impairment: a 1-year longitudinal study. Neurol Sci Off
899 J Ital Neurol Soc Ital Soc Clin Neurophysiol. 2020;41:57–63.

900 74. Sanguinetti E, Collado MC, Marrachelli VG, Monleon D, Selma-Royo M, Pardo-Tendero
901 MM, et al. Microbiome-metabolome signatures in mice genetically prone to develop dementia,
902 fed a normal or fatty diet. Sci Rep. 2018;8:4907.

903 75. Liu J, Zhang T, Wang Y, Si C, Wang X, Wang R-T, et al. Baicalin ameliorates
904 neuropathology in repeated cerebral ischemia-reperfusion injury model mice by remodeling
905 the gut microbiota. Aging. 2020;12:3791–806.

906 76. Wang Q-J, Shen Y-E, Wang X, Fu S, Zhang X, Zhang Y-N, et al. Concomitant memantine
907 and Lactobacillus plantarum treatment attenuates cognitive impairments in APP/PS1 mice.
908 Aging. 2020;12:628–49.

909 77. Sawicka AK, Renzi G, Olek RA. The bright and the dark sides of L-carnitine
910 supplementation: a systematic review. J Int Soc Sports Nutr. 2020;17:49.

911 78. Chung SJ, Rim JH, Ji D, Lee S, Yoo HS, Jung JH, et al. Gut microbiota-derived metabolite
912 trimethylamine N-oxide as a biomarker in early Parkinson's disease. Nutr 2020;83:111090.

913 79. Zhuang Z, Gao M, Yang R, Liu Z, Cao W, Huang T. Causal relationships between gut
914 metabolites and Alzheimer's disease: a bidirectional Mendelian randomization study.
915 Neurobiol Aging. 2020;

916 80. Li D, Ke Y, Zhan R, Liu C, Zhao M, Zeng A, et al. Trimethylamine-N-oxide promotes brain
917 aging and cognitive impairment in mice. Aging Cell. 2018;17:e12768.

918 81. Papandreou C, Moré M, Bellamine A. Trimethylamine N-Oxide in Relation to
919 Cardiometabolic Health-Cause or Effect? Nutrients. 2020;12.

920 82. Zeisel SH. Dietary choline: biochemistry, physiology, and pharmacology. Annu Rev Nutr.
921 1981;1:95–121.

922 83. Lundstrom RC, Racicot LD. Gas chromatographic determination of dimethylamine and
923 trimethylamine in seafoods. J Assoc Off Anal Chem. 1983;66:1158–63.

924 84. Zeng L-F, Cao Y, Liang W-X, Bao W-H, Pan J-K, Wang Q, et al. An exploration of the role
925 of a fish-oriented diet in cognitive decline: a systematic review of the literature. Oncotarget.
926 2017;8:39877–95.

927 85. Keenan TD, Agrón E, Mares JA, Clemons TE, Asten F van, Swaroop A, et al. Adherence
928 to a Mediterranean diet and cognitive function in the Age-Related Eye Disease Studies 1 & 2.
929 Alzheimers Dement. 2020;16:831–42.

930 86. Zhao W, Tang H, Yang X, Luo X, Wang X, Shao C, et al. Fish Consumption and Stroke
931 Risk: A Meta-Analysis of Prospective Cohort Studies. J Stroke Cerebrovasc Dis 2019;28:604–
932 11.

933 87. Zhang Y, Chen J, Qiu J, Li Y, Wang J, Jiao J. Intakes of fish and polyunsaturated fatty
934 acids and mild-to-severe cognitive impairment risks: a dose-response meta-analysis of 21
935 cohort studies. Am J Clin Nutr; 2016;103:330–40.

936 88. Cooper RE, Tye C, Kuntsi J, Vassos E, Asherson P. Omega-3 polyunsaturated fatty acid
937 supplementation and cognition: A systematic review and meta-analysis. J Psychopharmacol
938 2015;29:753–63.

939 89. Abdelhamid AS, Brown TJ, Brainard JS, Biswas P, Thorpe GC, Moore HJ, et al. Omega-
940 3 fatty acids for the primary and secondary prevention of cardiovascular disease. Cochrane
941 Database Syst Rev. 2018;11:CD003177.

942 90. Wall R, Ross RP, Fitzgerald GF, Stanton C. Fatty acids from fish: the anti-inflammatory
943 potential of long-chain omega-3 fatty acids. Nutr Rev. 2010;68:280–9.

944 91. Singh AK, Jiang Y. How does peripheral lipopolysaccharide induce gene expression in the
945 brain of rats? Toxicology. 2004;201:197–207.

946 92. Banks WA, Erickson MA. The blood-brain barrier and immune function and dysfunction.
947 Neurobiol Dis. 2010;37:26–32.

948 93. Gobbetti T, Cooray SN. Annexin A1 and resolution of inflammation: tissue repairing
949 properties and signalling signature. Biol Chem. 2016;397:981–93.

950 94. Nicholson JK, Holmes E, Kinross J, Burcelin R, Gibson G, Jia W, et al. Host-gut microbiota
951 metabolic interactions. Science. 2012;336:1262–7.

952 95. Needham BD, Kaddurah-Daouk R, Mazmanian SK. Gut microbial molecules in
953 behavioural and neurodegenerative conditions. Nat Rev Neurosci. 2020;21:717–31.

954

955 **Table 1.** BBB-associated genes whose expression was upregulated upon exposure of
956 hCMEC/D3 cells to TMAO.
957

Gene	Entrez ID	Description	Log_2 fold change	Category	P_{FDR}
TFRC	7037	Transferrin receptor	0.23	Transporter proteins	0.054
ABCC4	10257	ATP binding cassette subfamily C member 4	0.20	Transporter proteins	0.088
ANXA1	301	Annexin A1	0.16	Cell Adhesion/Junctional proteins/Cytoskeletal factors	0.088
CDH2	1000	Cadherin 2	0.31	Cell Adhesion/Junctional proteins/Cytoskeletal factors	0.095

958

959 **Table 2.** Daily consumption of TMAO and water in mice chronically treated with TMAO and/or
960 LPS. Data are mean ± standard deviation.
961

Variable	Sham-treated mice	LPS-treated mice	*P* value
TMAO intake (mg/day/mouse)	2.79 ± 0.38	2.82 ± 0.25	0.7
TMAO intake (mg/kg/mouse)	85.0 ± 11.4	88.9 ± 7.9	0.14
Water consumption (ml/day/mouse)	5.57 ± 0.8	5.64 ± 0.5	0.48

962

963 **FIGURE LEGENDS**

964 **Fig. 1.** Effects of TMAO and TMA on integrity of hCMEC/D3 cell monolayers. (A) Assessment
965 of paracellular permeability of hCMEC/D3 monolayers to a 70 kDa FITC-dextran tracer
966 following treatment for 24 h with varying doses of TMA (0.4 – 40 μM) or TMAO (4 – 4000 μM).
967 Data are expressed as mean ± s.e.m., *n*=4 independent experiments. (B) Assessment of
968 TEER of hCMEC/D3 monolayers to a 70kDa FITC-dextran tracer following treatment for 24 h
969 with varying doses of TMA (0.4 – 40 μM) or TMAO (4 – 4000 μM). Data are expressed as
970 mean ± s.e.m., *n*=4 independent experiments. (C) Adhesion of U937 monocytic cells to TNFα-
971 stimulated hCMEC/D3 monolayers (10 ng/ml, 16 h) that had been treated or not for 24 h with
972 0.4 μM TMA or 40 μM TMAO. Data are expressed as mean ± s.e.m., *n*=3 independent
973 experiments.

974

975 **Fig. 2.** Effects of TMA and TMAO on gene expression in hCMEC/D3 cells. (A) Heatmap
976 showing expression of the 49 genes found to be significantly (P_{FDR}<0.1) differentially
977 expressed upon exposure of hCMEC/D3 cells to 0.4 μM TMA (*n*=5 per group). (B) Heatmap
978 showing expression of the 440 genes found to be significantly (P_{FDR}<0.1) differentially
979 expressed upon exposure of hCMEC/D3 cells to 40 μM TMAO (*n*=5 per group). (C) Biological
980 processes associated with genes found to be significantly upregulated (*n*=39) or
981 downregulated (*n*=10) upon exposure of cells to TMA. (D) Biological processes of genes found
982 to be significantly upregulated (*n*=341) or downregulated (*n*=99) upon exposure of cells to
983 TMAO. Images in (C, D) shown based on Enrichr *P* value ranking from GO analysis. (E)
984 Topological analysis of the KEGG networks associated with the 440 genes whose expression
985 was significantly affected upon exposure of cells to TMAO (blue, significantly downregulated;
986 red, significantly upregulated); genes of similar cellullar role are highlighted. (F) Confocal
987 microscopic analysis of expression of fibrillar actin (F-actin) and the tight junction component
988 zonula occludens-1 (ZO-1) in hCMEC/D3 cells following treatment for 24 h with 0.4 μM TMA
989 or 40 μM TMAO. Images are representative of at least three independent experiments.

990

991 **Fig. 3.** Annexin A1 (ANXA1) signalling mediates effects of TMAO on hCMEC/D3 cells. (A)
992 Total cellular expression of ANXA1 in hCMEC/D3 cells treated for 24 h with 0.4 μM TMA or
993 40 μM TMAO. Data are expressed as mean ± s.e.m., *n*=5-7 independent experiments. (B)
994 Medium ANXA1 content of hCMEC/D3 monolayers treated for 24 h with 0.4 μM TMA or 40
995 μM TMAO. Data are expressed as mean ± s.e.m., *n*=7 independent experiments. (C)
996 Assessment of paracellular permeability of monolayers of wild-type hCMEC/D3 cells, or
997 hCMEC/D3 cells stably transfected with either a scramble shRNA sequence, or one of three
998 shRNA sequences targeting ANXA1 (clone 57/61 – 20.6 ± 5.6% reduction, clone 60A – 47.3

999 ± 1.5% reduction, clone 60B – 67.5 ± 1.1% reduction) to a 70kDa FITC-dextran tracer following
1000 treatment for 24 h with 40 μM TMAO. Data are expressed as mean ± s.e.m., *n*=4 independent
1001 experiments. (D) Assessment of TEER of monolayers of wild-type hCMEC/D3 cells, or
1002 hCMEC/D3 cells stably transfected with either a scramble shRNA sequence, or one of three
1003 shRNA sequences targeting ANXA1 (clone 57/61 – 20.6 ± 5.6% reduction, clone 60A – 47.3
1004 ± 1.5% reduction, clone 60B – 67.5 ± 1.1% reduction) following treatment for 24 h with 40 μM
1005 TMAO. Data are expressed as mean ± s.e.m., *n*=4 independent experiments. (E) Assessment
1006 of paracellular permeability of hCMEC/D3 cells to a 70kDa FITC-dextran tracer following
1007 treatment for 24 h with 40 μM TMAO, with or without 10 min pre-treatment with the FPR2
1008 antagonist WRW_4 (10 μM). Data are expressed as mean ± s.e.m., *n*=3 independent
1009 experiments. (F) Assessment of TEER of hCMEC/D3 cells following treatment for 24 h with
1010 40 μM TMAO, with or without 10 min pre-treatment with the FPR2 antagonist WRW_4 (10 μM).
1011 Data are expressed as mean ± s.e.m., *n*=3 independent experiments.
1012
1013 **Fig. 4.** Acute treatment with TMAO promotes BBB integrity *in vivo*. (A) Extravasation of Evans
1014 blue dye into brain parenchyma over a 1 h period in 2-month-old male C57Bl/6J mice following
1015 i.p. injection of 1.8 mg/kg TMAO for 2 h, 6 h or 24 h *vs.* a saline injected control. Data are
1016 normalised to plasma Evans blue content, and are expressed as mean ± s.e.m., *n*=5-6 mice.
1017 (B) Extravasation of Evans blue dye into brain parenchyma over a 1 h period in 2-month-old
1018 male C57Bl/6J mice following i.p. injection of saline or E. coli O111:B4 LPS (3 mg/kg) with or
1019 without subsequent i.p. injection of 1.8 mg/kg TMAO according to the schedule shown. Data
1020 are normalised to plasma Evans blue content, and are expressed as mean ± s.e.m., *n*=4-6
1021 mice.
1022
1023 **Fig. 5.** Acute exposure of mice to TMAO significantly alters the whole brain transcriptome. (A)
1024 Heatmap showing expression of the 76 genes found to be significantly (P_{FDR}<0.1) differentially
1025 expressed in the mouse brain after 2 h exposure to 1.8 mg/kg TMAO (*n*=3 per group). Data
1026 were scaled by row. (B) Over-representation analysis (Enrichr) showing KEGG pathways
1027 associated with the 76 genes. (C) Comparative analysis of significantly differentially expressed
1028 genes identified groupings associated with distinct biological functions. (D) Among the 197
1029 BBB-specific genes identified in the data set, only *App* and *Cpe* were significantly (P_{FDR}<0.1)
1030 differentially expressed in the mouse brain after 2 h exposure to TMAO. Data are shown as
1031 mean ± s.d, *n*=3 per group. Individual data points are not shown due to the negligible values
1032 of the s.d.
1033
1034 **Fig. 6.** Effect of long-term TMAO exposure on BBB integrity and cognitive function of mice in

1035 conjunction with sub-acute inflammatory challenge. (A) Body weight gain in mice treated with
1036 TMAO through their drinking water (0.5 mg/ml) over 2 months, combined with a chronic low
1037 dose administration of LPS (0.5 mg/kg/week, i.p.). Data are expressed as mean ± s.e.m., *n*=8
1038 mice, columns with different letters are significantly different at *P*<0.05. (B) Cerebellar
1039 permeability index to sodium fluorescein 2h following administration in animals previously
1040 treated with TMAO through their drinking water (0.5 mg/ml) over 2 months, combined with a
1041 chronic low dose administration of LPS (0.5 mg/kg/week, i.p.). Data are expressed as mean
1042 ± s.e.m., *n*=8 mice, columns with different letters are significantly different at *P*<0.05. (C)
1043 Typical confocal microscopic images of perivascular IgG deposition in male C57Bl/6J mice
1044 treated with TMAO through their drinking water (0.5 mg/ml) over 2 months, combined with a
1045 chronic low dose administration of LPS (0.5 mg/kg/week, i.p.). *Griffonia simplicifolia* isolectin
1046 B_4 (red) defines endothelial cells, areas of IgG deposition (white) are highlighted by arrow
1047 heads. (D) Distance travelled, (E) movement speed and (F) percentage of time in the centre
1048 as measured in the OFT in animals previously treated with TMAO through their drinking water
1049 (0.5 mg/ml) over 2 months, combined with a chronic low dose administration of LPS (0.5
1050 mg/kg/week, i.p.). Data are expressed as mean ± s.e.m., *n*=8 mice. (G) Novel object
1051 discrimination index, calculated as described in Methods, of animals previously treated with
1052 TMAO through their drinking water (0.5 mg/ml) over 2 months, combined with a chronic low
1053 dose administration of LPS (0.5 mg/kg/week, i.p.). Data are expressed as mean ± s.e.m., *n*=8
1054 mice, columns with different letters are significantly different at *P*<0.05. (H) Percentage of
1055 spontaneous alternation and (I) total distance travelled in the Y-maze test for animals
1056 previously treated with TMAO through their drinking water (0.5 mg/ml) over 2 months,
1057 combined with a chronic low dose administration of LPS (0.5 mg/kg/week, i.p.). Data are
1058 expressed as mean ± s.e.m., *n*=8 mice.
1059
1060 **Fig. 7.** Effects of long-term TMAO exposure upon astrocytes and microglia in the entorhinal
1061 cortex and hippocampus of mice in conjunction with sub-acute inflammatory challenge. (A)
1062 Typical immunohistochemical staining of GFAP+ astrocytes in the entorhinal cortex of mice
1063 previously treated with TMAO through their drinking water (0.5 mg/ml) over 2 months,
1064 combined with a chronic low dose administration of LPS (0.5 mg/kg/week, i.p.). Scale bar =
1065 40 μm. (B) Typical immunohistochemical staining of Iba1+ microglia in the entorhinal cortex
1066 of mice previously treated with TMAO through their drinking water (0.5 mg/ml) over 2 months,
1067 combined with a chronic low dose administration of LPS (0.5 mg/kg/week, i.p.), scale bar = 40
1068 μm. (C) Astrocyte and microglial primary process number and in the entorhinal cortex of mice
1069 previously treated with TMAO through their drinking water (0.5 mg/ml) over 2 months,
1070 combined with a chronic low dose administration of LPS (0.5 mg/kg/week, i.p.). Data are
1071 expressed as mean ± s.e.m., *n*=4 mice. (D) Astrocyte and microglial density in the entorhinal

1072 cortex of mice previously treated with TMAO through their drinking water (0.5 mg/ml) over 2
1073 months, combined with a chronic low dose administration of LPS (0.5 mg/kg/week, i.p.). Data
1074 are expressed as mean ± s.e.m., *n*=4 mice. (E) Typical immunohistochemical staining of
1075 GFAP+ astrocytes in the CA1 region of the hippocampus of mice previously treated with
1076 TMAO through their drinking water (0.5 mg/ml) over 2 months, combined with a chronic low
1077 dose administration of LPS (0.5 mg/kg/week, i.p.). Scale bar = 40 μm (F) Typical
1078 immunohistochemical staining of Iba1+ microglia in the CA1 region of the hippocampus of
1079 mice previously treated with TMAO through their drinking water (0.5 mg/ml) over 2 months,
1080 combined with a chronic low dose administration of LPS (0.5 mg/kg/week, i.p.), scale bar = 40
1081 μm. (G) Astrocyte and microglial primary process number in the CA1 region of the
1082 hippocampus of mice previously treated with TMAO through their drinking water (0.5 mg/ml)
1083 over 2 months, combined with a chronic low dose administration of LPS (0.5 mg/kg/week, i.p.).
1084 Data are expressed as mean ± s.e.m., *n*=4 mice. (H) Astrocyte and microglial density in the
1085 in the CA1 region of the hippocampus of mice previously treated with TMAO through their
1086 drinking water (0.5 mg/ml) over 2 months, combined with a chronic low dose administration of
1087 LPS (0.5 mg/kg/week, i.p.). Data are expressed as mean ± s.e.m., *n*=4 mice.
1088

Figure 1

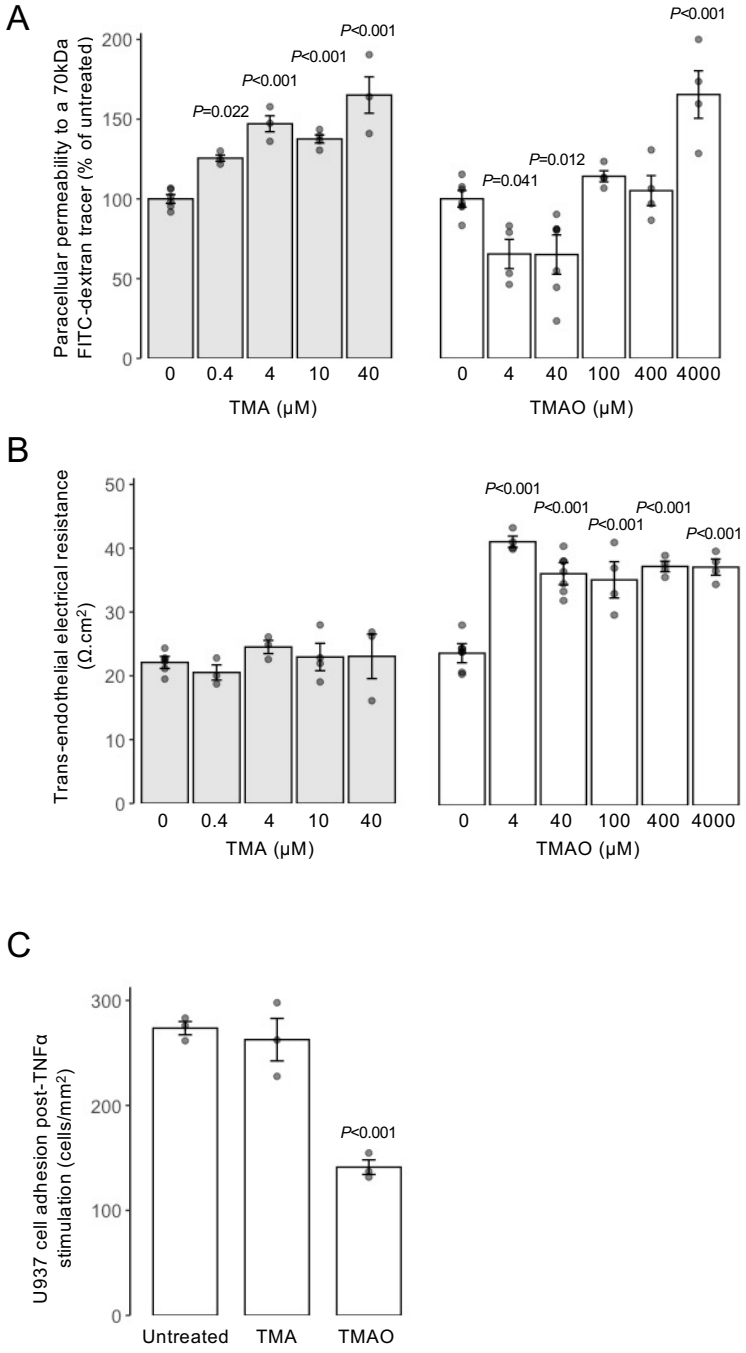
A
Paracellular permeability to a 70kDa FITC-dextran tracer (% of untreated)
200
150
100
50
0
P=0.022
P<0.001
P<0.001
P<0.001
0
0.4
4
10
40
TMA (µM)
P=0.041
P=0.012
P<0.001
0
4
40
100
400
4000
TMAO (µM)
B
Trans-endothelial electrical resistance (Ω.cm²)
50
40
30
20
10
0
0
0.4
4
10
40
TMA (µM)
P<0.001
P<0.001
P<0.001
P<0.001
P<0.001
0
4
40
100
400
4000
TMAO (µM)
C
U937 cell adhesion post-TNFα stimulation (cells/mm²)
300
200
100
0
P<0.001
Untreated
TMA
TMAO

Figure 2

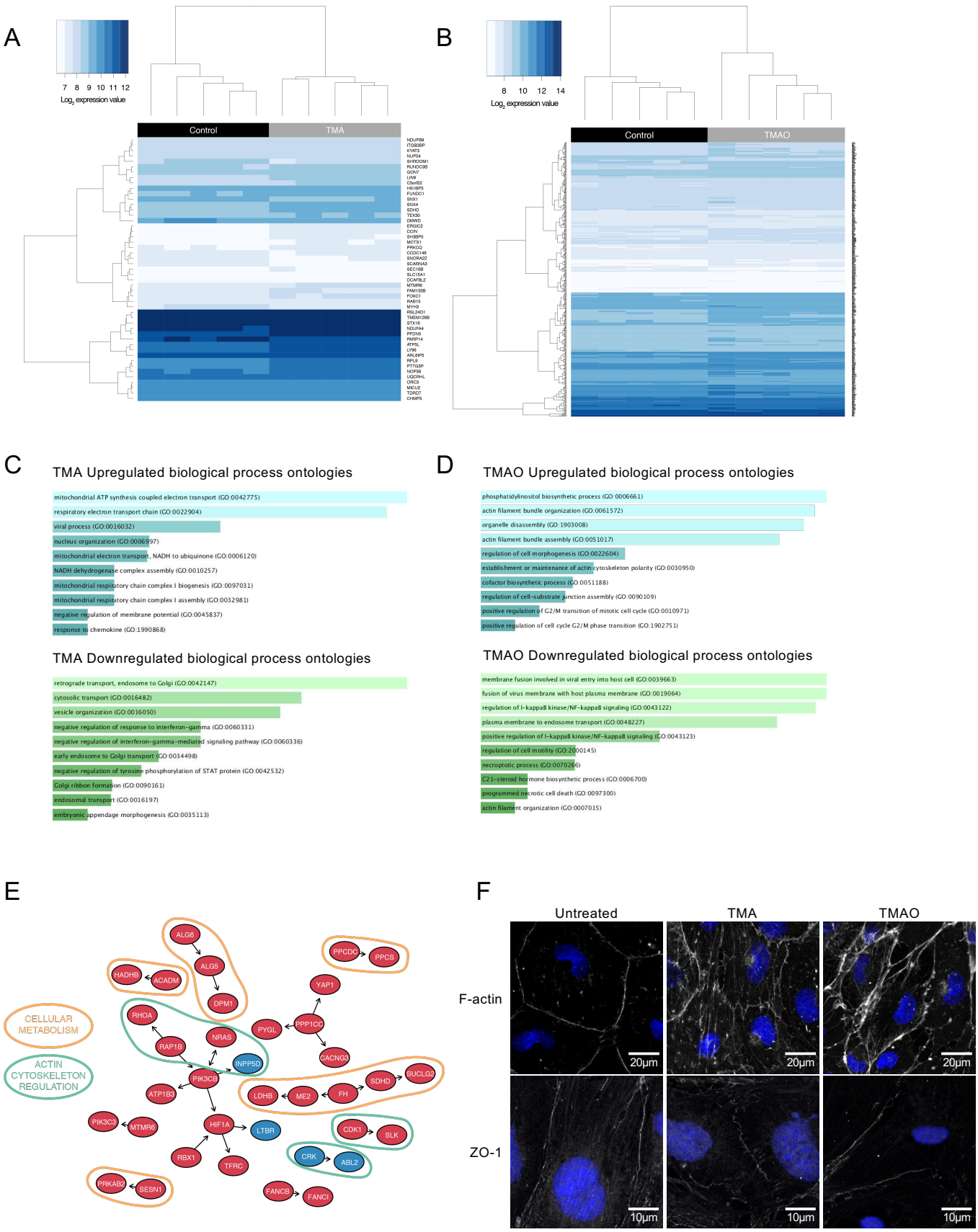
A
7 8 9 10 11 12
Log2 expression value
Control
TMA
B
8 10 12 14
Log2 expression value
Control
TMAO
C
TMA Upregulated biological process ontologies
mitochondrial ATP synthesis coupled electron transport (GO:0042775)
respiratory electron transport chain (GO:0022904)
viral process (GO:0016032)
nucleus organization (GO:0006997)
mitochondrial electron transport, NADH to ubiquinone (GO:0006120)
NADH dehydrogenase complex assembly (GO:0010257)
mitochondrial respiratory chain complex I biogenesis (GO:0097031)
mitochondrial respiratory chain complex I assembly (GO:0032981)
negative regulation of membrane potential (GO:0045837)
response to chemokine (GO:1990868)
TMA Downregulated biological process ontologies
retrograde transport, endosome to Golgi (GO:0042147)
cytosolic transport (GO:0016482)
vesicle organization (GO:0016050)
negative regulation of response to interferon-gamma (GO:0060331)
negative regulation of interferon-gamma-mediated signaling pathway (GO:0060336)
early endosome to Golgi transport (GO:0034498)
negative regulation of tyrosine phosphorylation of STAT protein (GO:0042532)
Golgi ribbon formation (GO:0090161)
endosomal transport (GO:0016197)
embryonic appendage morphogenesis (GO:0035113)
D
TMAO Upregulated biological process ontologies
phosphatidylinositol biosynthetic process (GO:0006661)
actin filament bundle organization (GO:0061572)
organelle disassembly (GO:1903008)
actin filament bundle assembly (GO:0051017)
regulation of cell morphogenesis (GO:0022604)
establishment or maintenance of actin cytoskeleton polarity (GO:0030950)
cofactor biosynthetic process (GO:0051188)
regulation of cell-substrate junction assembly (GO:0090109)
positive regulation of G2/M transition of mitotic cell cycle (GO:0010971)
positive regulation of cell cycle G2/M phase transition (GO:1902751)
TMAO Downregulated biological process ontologies
membrane fusion involved in viral entry into host cell (GO:0039663)
fusion of virus membrane with host plasma membrane (GO:0019064)
regulation of I-kappaB kinase/NF-kappaB signaling (GO:0043122)
plasma membrane to endosome transport (GO:0048227)
positive regulation of I-kappaB kinase/NF-kappaB signaling (GO:0043123)
regulation of cell motility (GO:2000145)
necroptotic process (GO:0070266)
C21-steroid hormone biosynthetic process (GO:0006700)
programmed necrotic cell death (GO:0097300)
actin filament organization (GO:0007015)
E
CELLULAR METABOLISM
ACTIN CYTOSKELETON REGULATION
ALG6
ALG5
DPM1
HADHB
ACADM
PPCDC
PPCS
YAP1
RHOA
RAP1B
NRAS
PYGL
PPP1CC
CACNG5
INPP5D
PIK3CB
ATP1B3
SDHD
SUCLG2
LDHB
ME2
FH
PIK3C3
MTMR6
HIF1A
LTBR
CDK1
SLK
RBX1
TFRC
CRK
ABL2
PRKAB2
SESN1
FANCB
FANCI
F
Untreated
TMA
TMAO
F-actin
ZO-1
20μm
10μm

Figure 3

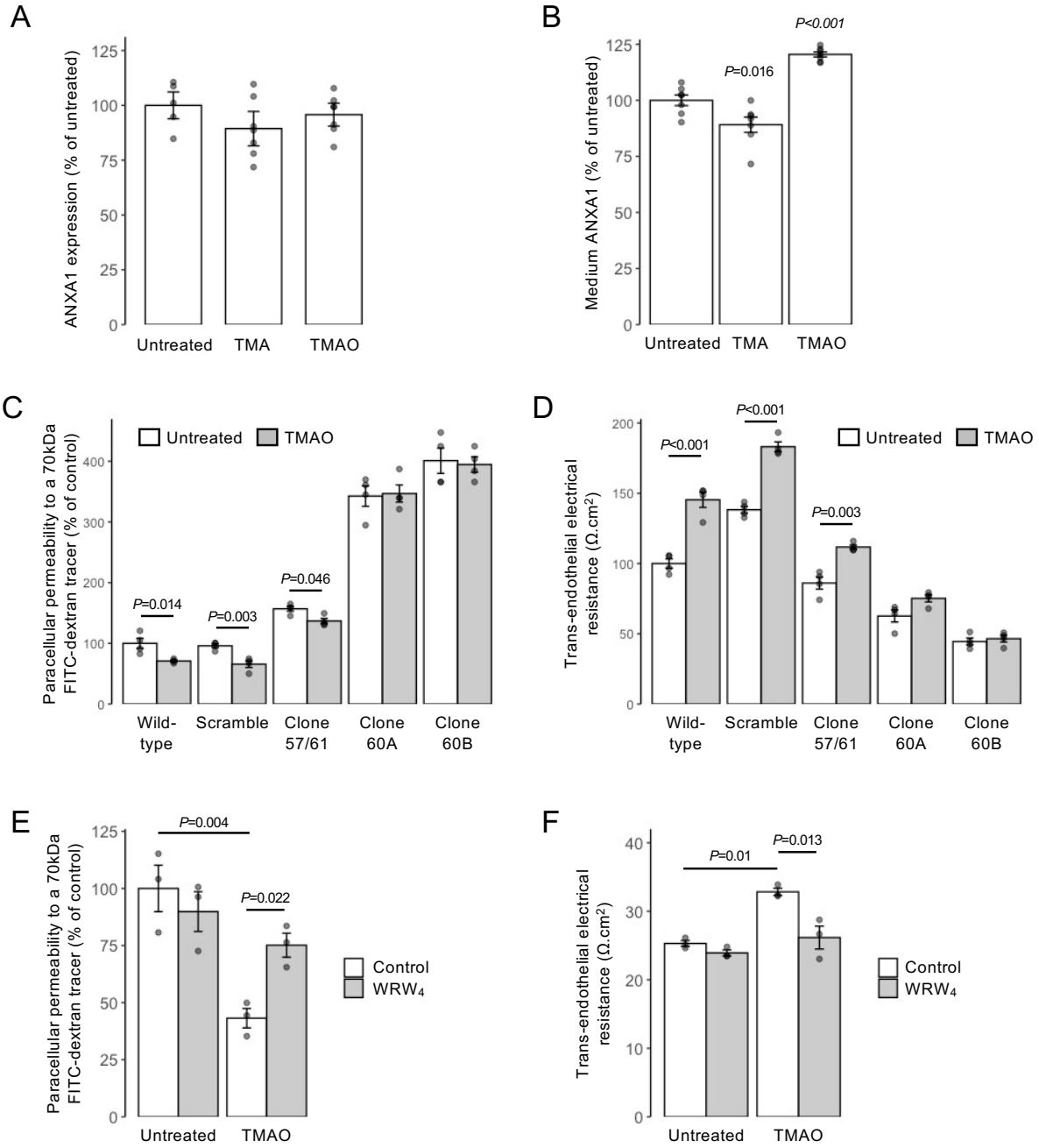
A
ANXA1 expression (% of untreated)
125
100
75
50
25
0
Untreated
TMA
TMAO
B
Medium ANXA1 (% of untreated)
P<0.001
P=0.016
Untreated
TMA
TMAO
C
Paracellular permeability to a 70kDa FITC-dextran tracer (% of control)
Untreated
TMAO
P=0.014
P=0.003
P=0.046
Wild-type
Scramble
Clone 57/61
Clone 60A
Clone 60B
D
Trans-endothelial electrical resistance (Ω.cm²)
P<0.001
P<0.001
P=0.003
Untreated
TMAO
Wild-type
Scramble
Clone 57/61
Clone 60A
Clone 60B
E
Paracellular permeability to a 70kDa FITC-dextran tracer (% of control)
P=0.004
P=0.022
Control
WRW4
Untreated
TMAO
F
Trans-endothelial electrical resistance (Ω.cm²)
P=0.01
P=0.013
Control
WRW4
Untreated
TMAO

Figure 4

A

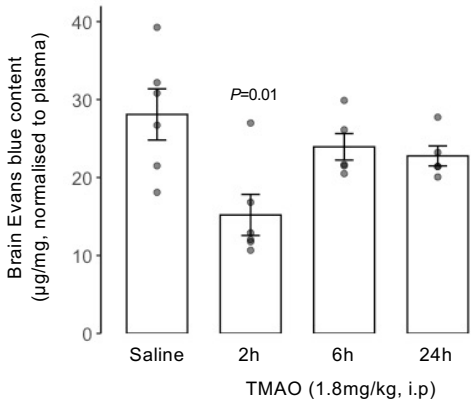
Brain Evans blue content
(µg/mg, normalised to plasma)
40
30
20
10
0
P=0.01
Saline
2h
6h
24h
TMAO (1.8mg/kg, i.p)

B

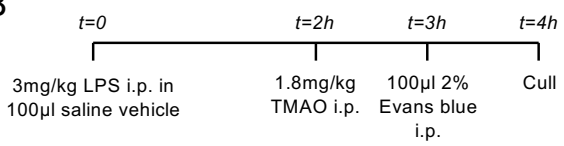
t=0
t=2h
t=3h
t=4h
3mg/kg LPS i.p. in
100µl saline vehicle
1.8mg/kg
TMAO i.p.
100µl 2%
Evans blue
i.p.
Cull

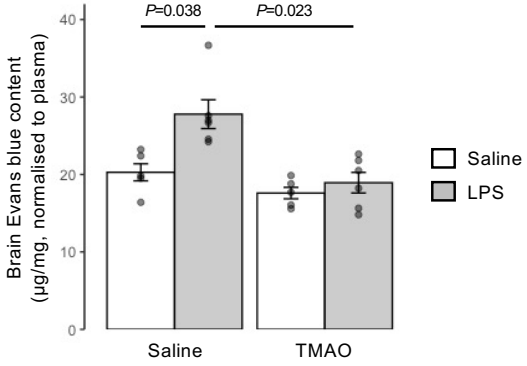
Brain Evans blue content
(µg/mg, normalised to plasma)
40
30
20
10
0
P=0.038
P=0.023
Saline
TMAO
Saline
LPS

Figure 5

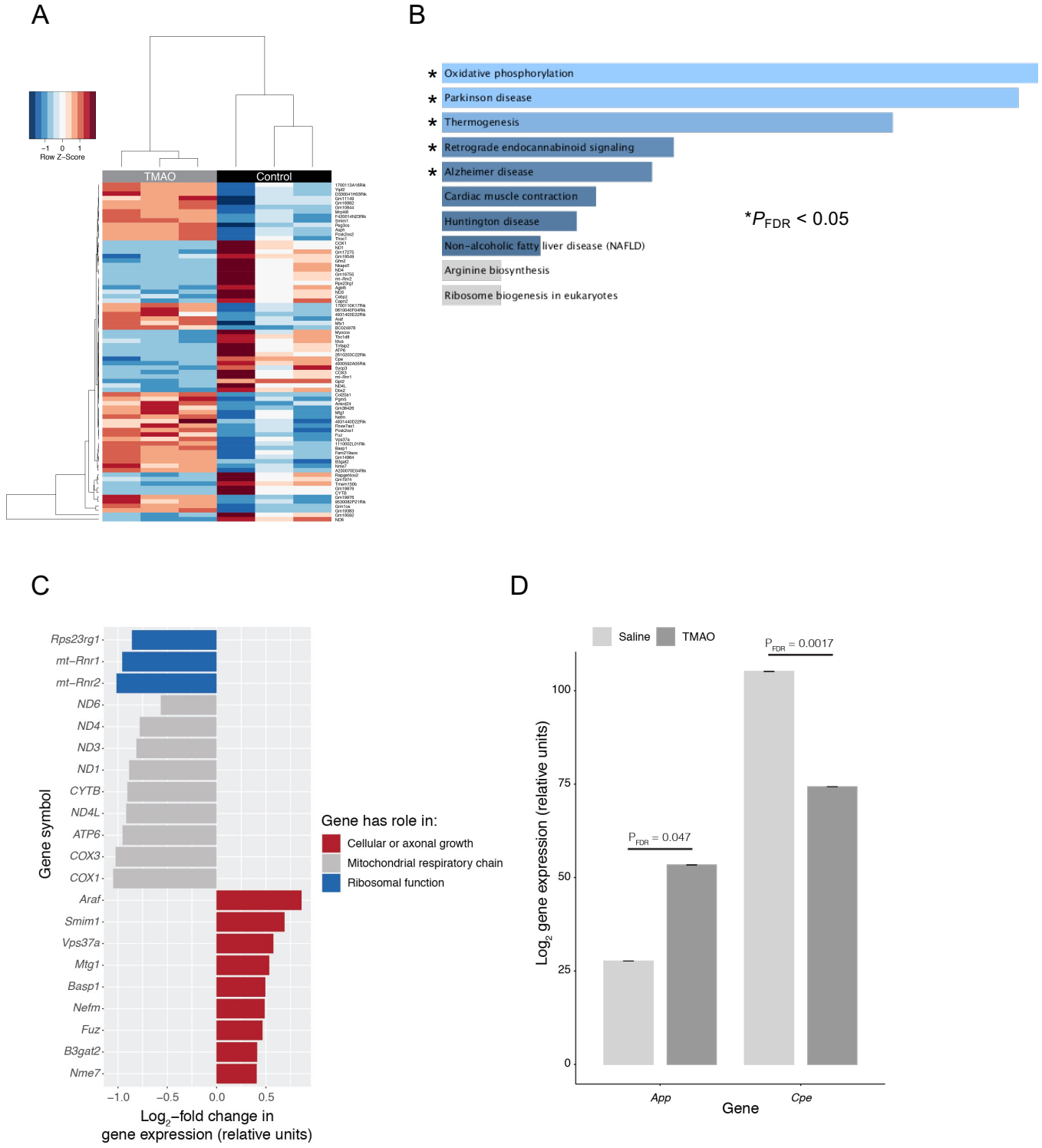
A
−1 0 1
Row Z-Score
TMAO
Control
B
Oxidative phosphorylation
Parkinson disease
Thermogenesis
Retrograde endocannabinoid signaling
Alzheimer disease
Cardiac muscle contraction
Huntington disease
Non-alcoholic fatty liver disease (NAFLD)
Arginine biosynthesis
Ribosome biogenesis in eukaryotes
*P_FDR < 0.05
C
Rps23rg1
mt−Rnr1
mt−Rnr2
ND6
ND4
ND3
ND1
CYTB
ND4L
ATP6
COX3
COX1
Araf
Smim1
Vps37a
Mtg1
Basp1
Nefm
Fuz
B3gat2
Nme7
Gene symbol
−1.0 −0.5 0.0 0.5
Log2−fold change in gene expression (relative units)
Gene has role in:
Cellular or axonal growth
Mitochondrial respiratory chain
Ribosomal function
D
Saline
TMAO
P_FDR = 0.0017
P_FDR = 0.047
Log2 gene expression (relative units)
0 25 50 75 100
App
Cpe
Gene

Figure 6

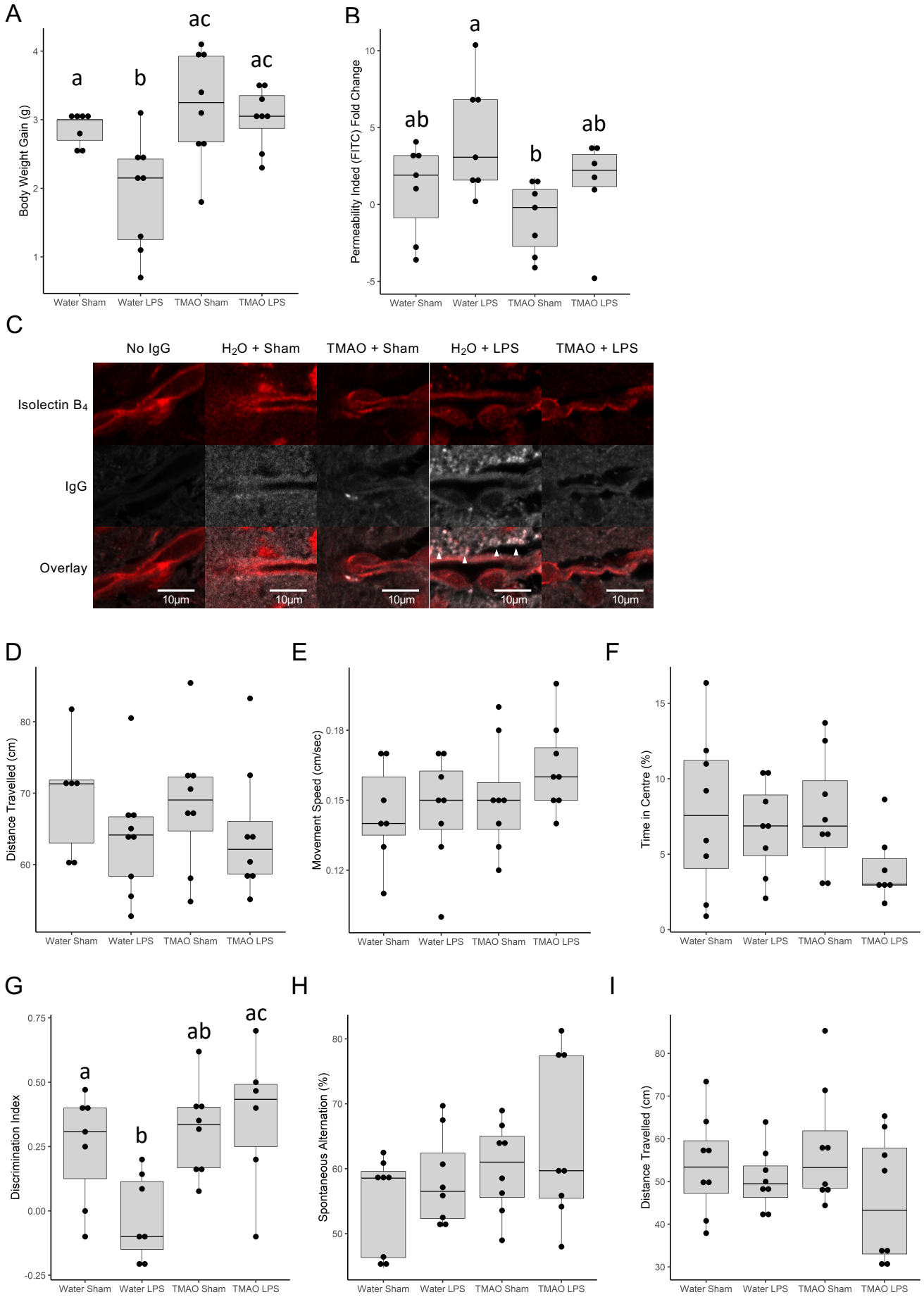
A
Body Weight Gain (g)
a
b
ac
ac
Water Sham
Water LPS
TMAO Sham
TMAO LPS
B
Permeability Inded (FITC) Fold Change
ab
a
b
ab
C
No IgG
H2O + Sham
TMAO + Sham
H2O + LPS
TMAO + LPS
Isolectin B4
IgG
Overlay
10μm
D
Distance Travelled (cm)
E
Movement Speed (cm/sec)
F
Time in Centre (%)
G
Discrimination Index
a
b
ab
ac
H
Spontaneous Alternation (%)
I
Distance Travelled (cm)

Figure 7

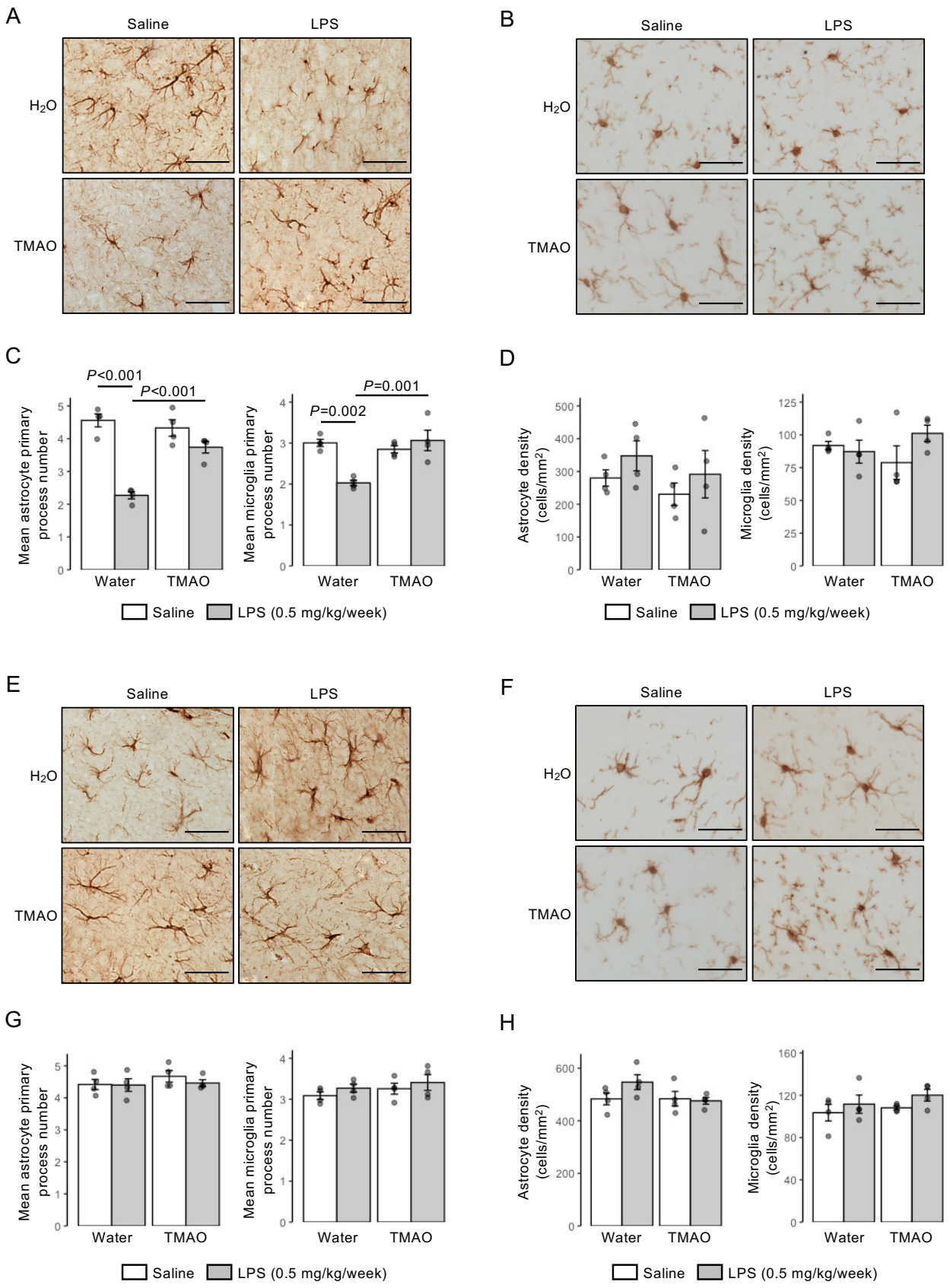
A
Saline
LPS
H2O
TMAO
B
Saline
LPS
H2O
TMAO
C
P<0.001
P<0.001
Mean astrocyte primary process number
Water
TMAO
P=0.001
P=0.002
Mean microglia primary process number
Water
TMAO
Saline
LPS (0.5 mg/kg/week)
D
Astrocyte density (cells/mm2)
Water
TMAO
Microglia density (cells/mm2)
Water
TMAO
Saline
LPS (0.5 mg/kg/week)
E
Saline
LPS
H2O
TMAO
F
Saline
LPS
H2O
TMAO
G
Mean astrocyte primary process number
Water
TMAO
Mean microglia primary process number
Water
TMAO
Saline
LPS (0.5 mg/kg/week)
H
Astrocyte density (cells/mm2)
Water
TMAO
Microglia density (cells/mm2)
Water
TMAO
Saline
LPS (0.5 mg/kg/week)

Supplementary Information

Supplementary Fig. 1. Confirmation of ANXA1 targeting and knock-down in hCMEC/D3 cells stably transfected with appropriate shRNA sequences. (A) Typical flow cytometric profiles of wild-type cells, cells transfected with a scramble shRNA sequence and cells transfected with one of three ANXA1-targeting shRNA sequences, alongside unstained and second antibody controls. (B) Expression of ANXA1 in wild-type hCMEC/D3 cells, cells transfected with a scramble shRNA sequence and cells transfected with one of three ANXA1-targeting shRNA sequences. Data are expressed as mean ± s.e.m., *n*=4 independent experiments.

Supplementary Fig. 2. Neither TMAO nor TMA treatment affected the major endothelial efflux transporters BCRP or P-glycoprotein. (A-D) *In vitro* analysis revealed no significant effects of either TMAO or TMA upon BCRP (A, C) or P-glycoprotein (B, D) activity. Dashed lines represent Loess regression fits, with shading representing 95% confidence intervals. (E) hCMEC/D3 cell surface expression of BCRP was unaffected by 24 h exposure to TMA (0.4 μM) or TMAO (40 μM). Data are expressed as mean ± s.e.m., *n*=3 independent experiments. (F) hCMEC/D3 cell surface expression of P-glycoprotein was unaffected by 24 h exposure to TMA (0.4 μM) or TMAO (40 μM). Data are expressed as mean ± s.e.m., *n*=3 independent experiments.

Supplementary Fig. 3. *In vitro* (hCMEC/D3 cell) *FMO3* gene expression is unaffected by exposure to TMA (0.4 μM) or TMAO (40 μM). Dark blue lines represent the standard deviation (+/-). There was no statistically significant difference between TMA and the control, nor between TMAO and the control (Supplementary Tables 2 and 3). Individual data points are not shown due to the negligible values of the standard deviations.

Supplementary Fig. 4. Neither chronic low-dose LPS nor TMAO treatment significantly increases serum inflammatory cytokines. (A) Serum TNFα concentrations in male C57Bl/6J mice treated with TMAO through their drinking water (0.5 mg/ml) over 2 months, combined with a chronic low dose administration of LPS (0.5 mg/kg/week, i.p.). Data are expressed as mean ± s.e.m., *n*=7-8 mice. (B) Serum IL-

1β concentrations in male C57Bl/6J mice treated with TMAO through their drinking water (0.5 mg/ml) over 2 months, combined with a chronic low dose administration of LPS (0.5 mg/kg/week, i.p.). Data are expressed as mean ± s.e.m., *n*=7-8 mice.

The supplementary tables listed below are available from figshare (https://doi.org/10.6084/m9.figshare.13549334.v1).

Supplementary Table 1. Normalized microarray data for hCMEC/D3 treated or not with TMA (0.4 μM) or TMAO (40 μM)

Supplementary Table 2. Differential gene expression for control compared with TMA treatment, as assessed using LIMMA

Supplementary Table 3. Differential gene expression for control compared with TMAO treatment, as assessed using LIMMA

Supplementary Table 4. KEGG-based SPIA of genes whose expression was significantly affected by TMAO

Supplementary Table 5. GO (biological process) analysis of TMA-up-regulated genes as assessed using Enrichr

Supplementary Table 6. GO (biological process) analysis of TMA-down-regulated genes as assessed using Enrichr

Supplementary Table 7. GO (biological process) analysis of TMAO-up-regulated genes as assessed using Enrichr

Supplementary Table 8. GO (biological process) analysis of TMAO-down-regulated genes as assessed using Enrichr

Supplementary Table 9. Differential gene expression of BBB-associated genes (*in vitro* TMA treatment)

Supplementary Table 10. Differential gene expression of BBB-associated genes (*in vitro* TMAO treatment)

Supplementary Table 11. Differential gene expression in mouse brain for control compared with TMAO treatment, as assessed using DESeq2

Supplementary Table 12. Differential expression of BBB-associated genes in mouse brain for control compared with TMAO treatment, as assessed using DESeq2

Supplementary Figure 1

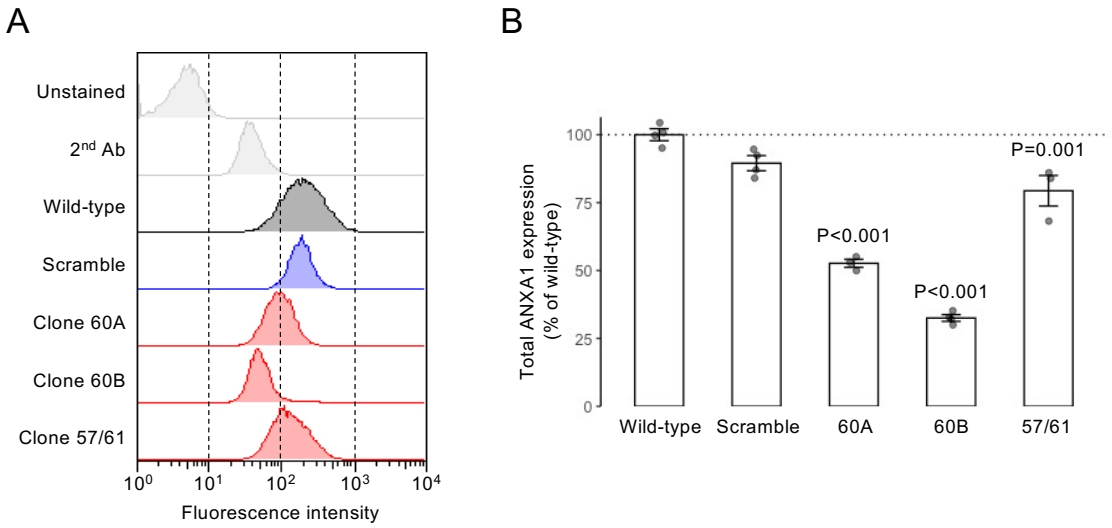

Supplementary Figure 2

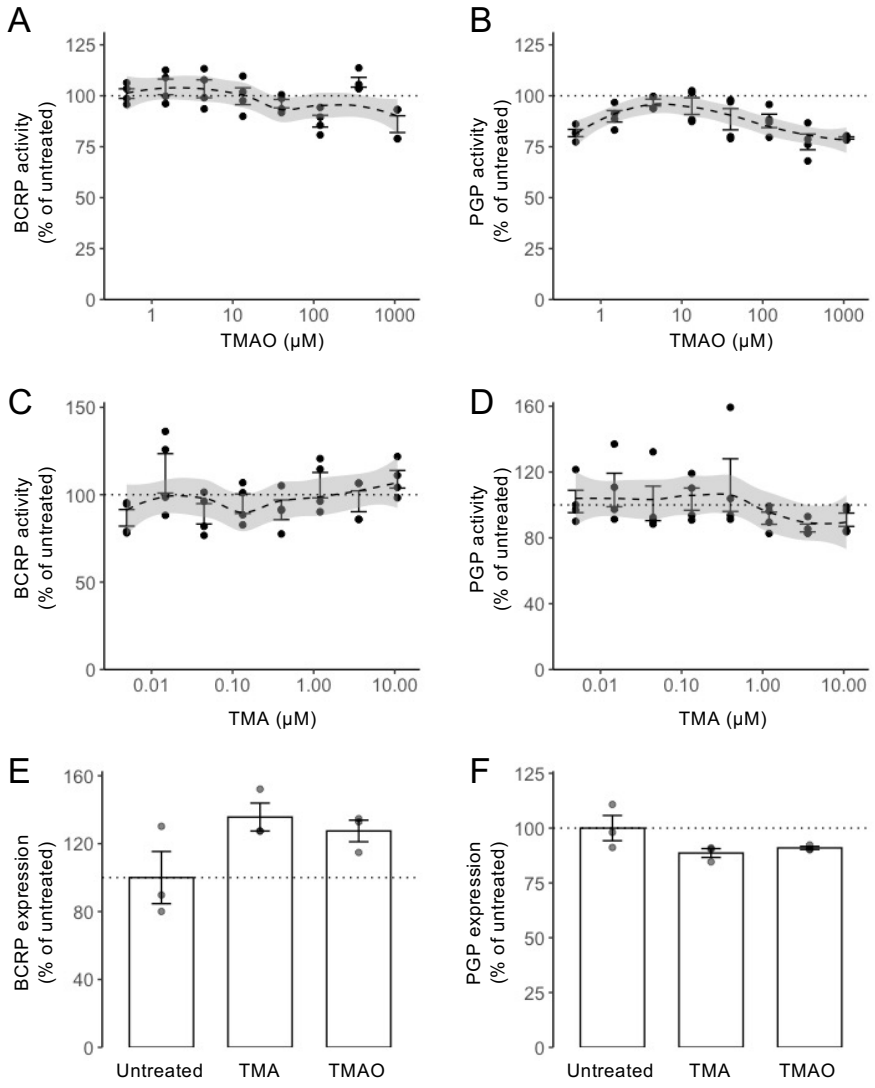

Supplementary Figure 3

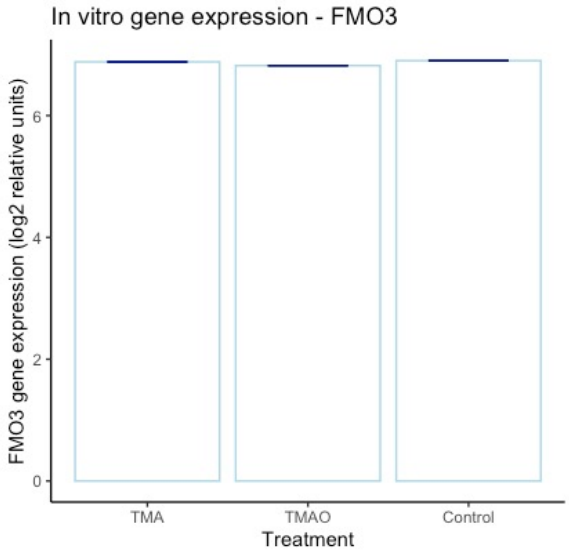
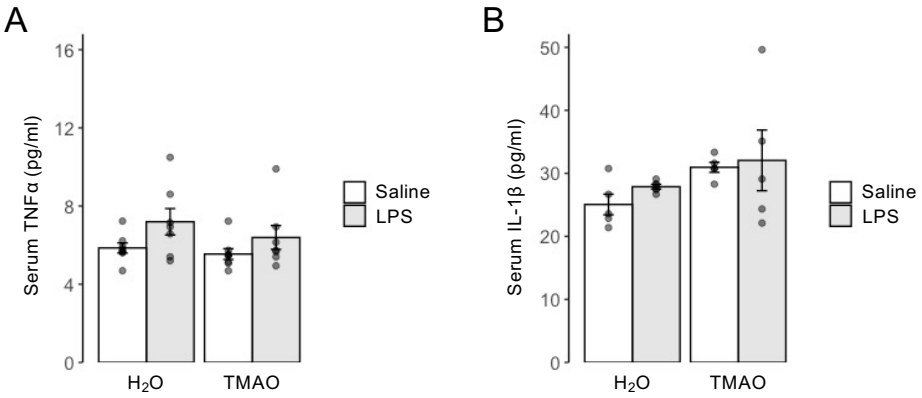
Supplementary Figure 4